Engineering cofactor and ligand binding in an artificial neuroglobin

by

LEI ZHANG

A dissertation submitted to the Graduate Faculty in Physics in partial fulfillment of the requirements for the degree of Doctor of Philosophy, The City University of New York.

2012

This manuscript has been read and accepted for the Graduate Faculty in Physics in satisfaction of the dissertation requirements for the degree of Doctor in Philosophy.

08/27/2012

Date

Prof. Ronald L. Koder

The Chair of Examining Committee

08/27/2012

Date

Prof. Steven G. Greenbaum

Executive Officer

Prof. Vikas Nanda

Prof. Marilyn Gunner

Prof. Ranajeet Ghose

Prof. Brian Gibney

(Supervisory committee)

THE CITY UNIVERSITY OF NEW YORK

ABSTRACT

Engineering cofactor and ligand binding in an artificial neuroglobin

by

LEI ZHANG

Advisor: Professor Ronald L. Koder

HP-7 is one artificial mutated oxygen transport protein, which operates via a mechanism akin to human neuroglobin and cytoglobin. This protein destabilizes one of two heme- ligating histidine residues by coupling histidine side chain ligation with the burial of three charged glutamate residues on the same helix. Replacement of these glutamate residues with alanine, which has a neutral hydrophobicity, slows gaseous ligand binding 22-fold, increases the affinity of the distal histidine ligand by a factor of thirteen, and decreases the binding affinity of carbon monoxide, a nonreactive oxygen analogue, three-fold. Paradoxically, it also decreases heme binding affinity by a factor of three in the reduced state and six in the oxidized state. Application of a two-state binding model, in which an initial pentacoordinate binding event is followed by a protein conformational change to hexacoordinate, provides insight into the mechanism of this seemingly counterintuitive result: the initial pentacoordinate encounter complex is significantly destabilized by the loss of the glutamate side chains, and the increased affinity for the distal histidine only partially compensates. These results point to the importance of considering each oxidation

and conformational state in the design of functional artificial proteins. We have also examined the effects these mutations have on function. The K_d of the nonnreactive oxygen analogue carbon monoxide (CO) is only decreased three-fold, despite the large increase in distal histidine affinity engendered by the 22-fold decrease in the histidine ligand off-rate. This is a result of the four-fold increase in affinity for CO binding to the pentacoordinate state. Oxygen binds to HP7 with a K_d of 117 μM, while the mutant rapidly oxidizes when exposed to oxygen. EPR analysis of both ferric hemoproteins demonstrates that the mutation increases disorder at the heme binding site. NMR-detected deuterium exchange demonstrates that the mutation causes a large increase in water penetration into the protein core. The inability of the mutant protein may thus either be due to increased water penetration, the large decrease in binding rate caused by the increase in distal histidine affinity, or a combination of the two factors.

Acknowledgement

I want to express my special thanks to my mentor Prof. Dr. Ronald L.Koder not only for giving me an opportunity to work in his lab but also for his encouragement, thoughtful guidance and belief in me. I greatly appreciate his timely contribution and unconditional commitment to this work. Prof. Koder I would like to say from deep core of my heart that without your help and guidance this work would not have been possible.

I owe thanks to my dissertation committee members: Prof. Brian Gibney from Brooklyn College, Prof. Marilyn Gunner and Prof. Ranajeet Ghose form City College for their time and input over the years. Special thanks to Hsin Wang, who helped and taught me NMR operation and analysis technology for my dissertation.

I would also like to thank my friends and lab mates Dr. Sunaina Singh, Dr. Gheevarghese Raju, Mr. Jeff Chaing, Mr. Andrew Mutter, Mr. Bernard Everson, Mr. Eskil Andersen, Mr. Joe Brisendine, Mr. Cooper French, Miss Sara Morsi.

Finally, I would like to thank my family especially to my parents Mr. Peifu Zhang and Mrs. Fenglian He for supporting me in pursuing my dreams.

Contents

Figures

Chapter 1: Introduction

Section 1.1: An overview of *de novo* protein design

As the technology for designing and inserting the specific active sites into the protein scaffold develops rapidly, designed enzymes have infinite potential for future industrial applications (1,2).Designed proteins have significant advantages over natural proteins. They can be designed to be utilized on a wide range of environmental conditions (2, 3). Proteins have been designed to exhibit more stable structure at a wide range of pH and even temperatures approaching 100^{o}C. As well as performing in extreme conditions, they can be engineered to perform a variety of reactions including those found in natural proteins as well as novel mechanisms. De novo designed proteins can provide a useful and easy platform to define and test the principles of protein engineering

De novo protein design has recently developed rapidly and utilized in studying of protein structure and function, estimate the protein's tertiary structure from the sequence; design simple protein following the fundamental principle of protein folding; test and refine our knowledge of the principle of protein fold and function. As the knowledge evolved, it should be possible to design the artificial enzymes, proteins and biometric polymers with specific properties and function.

Cytochrome P450 enzymes are widely utilized in industry as outstanding natural enzymes(6).

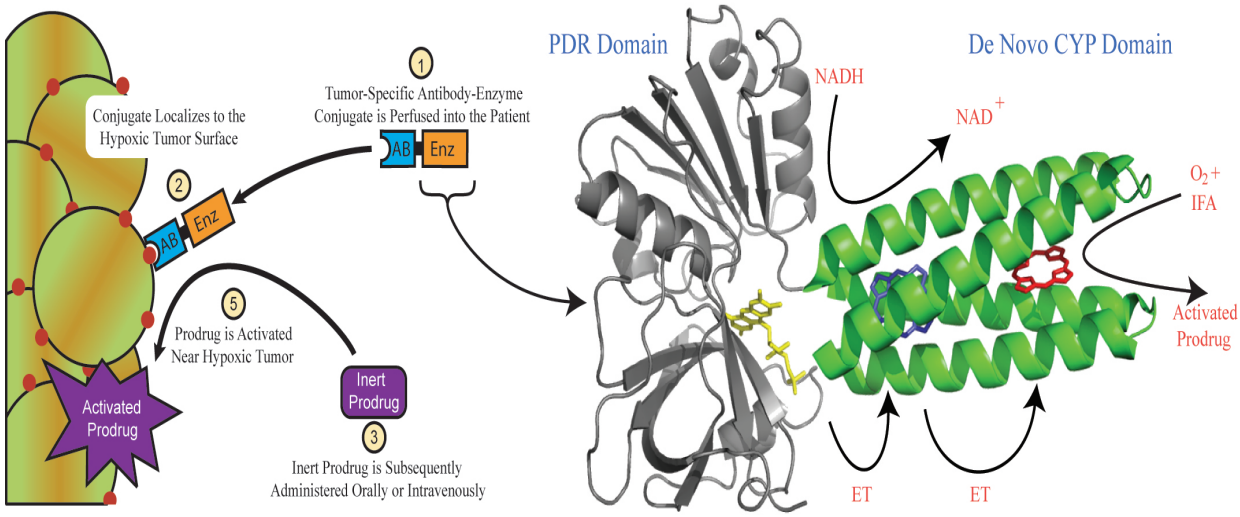

Figure 1.1 Antibody-enzyme prodrug therapy and enzyme structure

Antibody directed enzyme-prodrug therapy (ADEPT) employs an enzyme prodrug pair to directly target tumor cells. Using a covalently attached antibody to bring the enzyme to the tumor cells, the enzyme converts the inactive prodrug into an active, toxic drug only in the vicinity of the tumor. The activated drug kills tumor cells, leaving the rest of the body relatively unaffected. Currently the enzymes used in this form of cancer chemotherapy are natural or modified natural enzymes. Since there are endogenous homologues of these enzymes, the prodrugs are inappropriately activated by these human enzymes in other areas of the body. This promiscuous activation limits the dosage of these chemotherapeutic agents and thus limits their effectiveness as tumor fighting drugs. Designed proteins offer a way to avoid enzymes with endogenous homologues while increasing the dosage and effectiveness of the cancer killing drug.

Our goal is to create a de novo designed P450 enzyme capable of activating a prodrug. This enzyme will consist of two parts, a PDR domain and a de novo designed CYP domain with two binding sites: heme binding and gas binding. The PDR domain, taken from a bacterial reductase, uses NADH to provide sequential single electrons to CYP domain. The first electron goes to the heme. When O_2 binds the gas binding site, PDR provides a second electron. Both of the electrons are transferred to the prodrug to make the activated toxin.

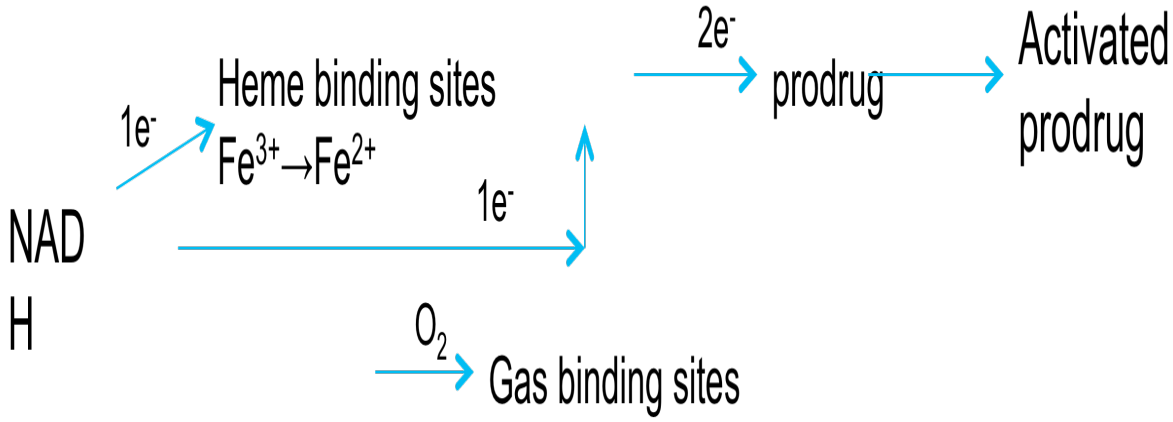

Figure 1.2 Enzyme-prodrug mechanism

The two binding sites have significant and important effects on electron transfer. The first and critical problem is how to design the two binding sites such that one can only bind gas while the other can only bind heme.

*protein design algorithm***:** There are four stages involved in the design of a functional designed protein (5):

1) Assemble a simple, generic protein framework, such as the appropriately sized helical bundle to support the cofactor binding and enzyme functions;
2) Insert the cofactor binding amino acids, changing a limited number of proximal helical amino acids to maintain the protein framework while accommodating cofactor binding sites.
3) Adjust the sequence for improved structure.
4) Test and redesign to refine the function.

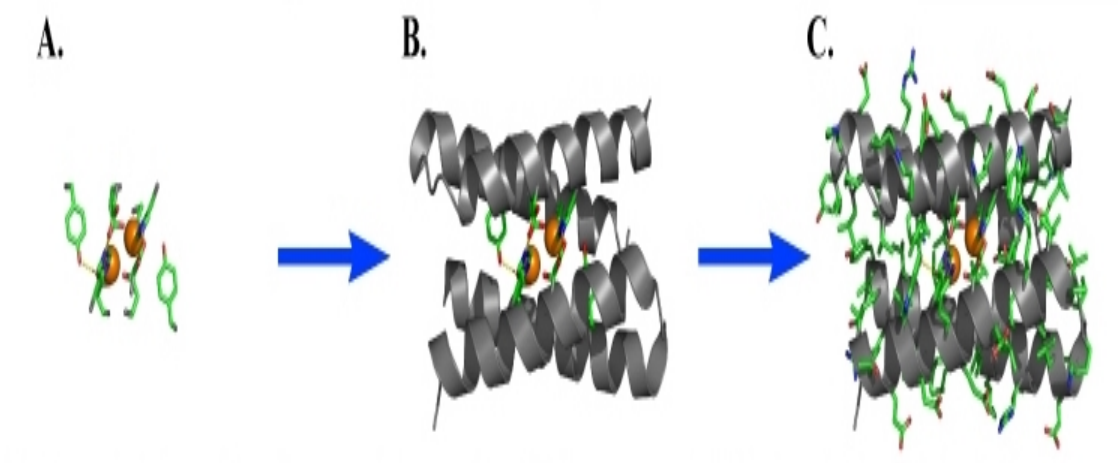

Figure 1.3 Protein design mechanism four-helix bundle was utilized as a framework, with the cofactor binding sites deriving from the PDB and/or computational analysis, locate this binding site in the four helix bundle, choose those proximal amino acids which will support the backbone and the keystone, and experimentally test to determine function and then begin optimizing the functionality(1).

Section 1.2: Binary patterning in *de novo* protein design.

About two decades ago the burial of hydrophobic area was discovered as the dominant force to form the protein folding. water-soluble To create the four-helix bundle we use as a framework, Ho and DeGrado first used binary patterning to design a four-helix bundle protein (7-9). Binary patterning relies on the simple principle that alpha-helix is consisting of alternately polar and nonpolar amino acid. Based on a two turn heptad repeat sequence of α-helix, they generated a series of peptides which have an alternating pattern of polar and nonpolar helix-forming residues, with the polar (E,K,D,Q,N) residues exposed and non-polar (L,A,F,I) residues in protein core.

In our work, we use the designed protein HP7(5)，whose sequence is

G EIWKQ HEDALQK FEEALNQ FED-LKQL GGSGCGSG

G EIWKQ HEDALQK FEEALNQ FED-LKQL

This protein was designed in the Dutton lab as follows:

Three repeats of the amino acid sequence **LEELLKK** were created:

G ELLKL LEELLKK LEELLKL LEELLKK L

With E and K exposed and L buried inside, which works alternately as $(a_{nonpolar}\text{-}b_{polar}\text{-}c_{polar}\text{-}d_{nonpolar}\text{-}e_{either}\text{-}f_{polar}\text{-}g_{either})_n$, and with an N-terminal CGGG sequence to restrict helical topologies to syn or anti.

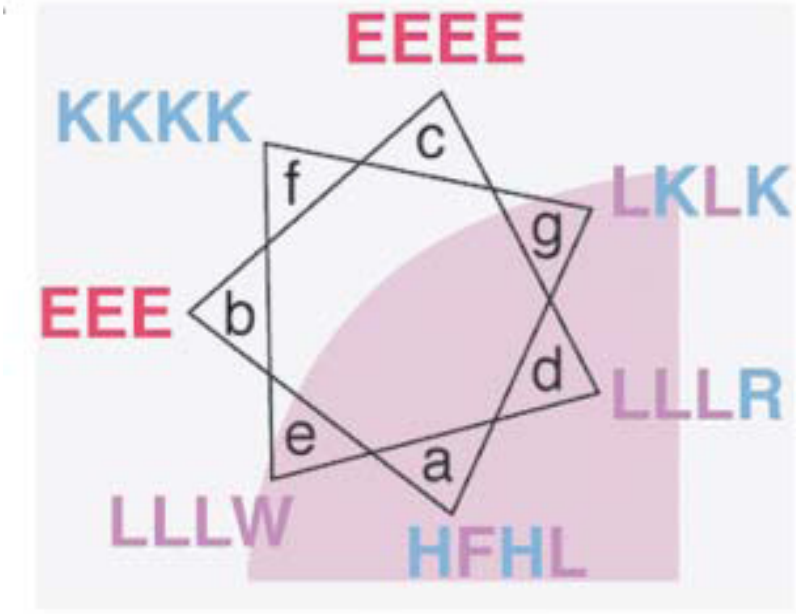

Figure 1.4 Binary patterning of helices bundle (Koder, R.L, Dutton, P.L (2006) Dalton Trans.25:3045-3051)

In order to be able to optically detect the protein, they replaced the e-position of each helix of the Tryptophan (W). Second, they replaced the 7, and 42-position leucines with histidine to bind the heme cofactor. In the natural protein there is a common amino acid phenylalanine (F) near hemes, so they replaced the 14-position L with F. The resulting sequence is:

G EIWKL HEELLKK FEELLKL HEELLKKL

To break the symmetry and distinguish the different heme binding sites, they replaced the interior leucine (d-position) with arginine(R).

G EIWKL HEELLKK FEELLKL HEERLKKL

To simplify the design they reduced the histidine from 4 to 2; and from a database analysis of natural bis-histidine heme protein they found that the helices must rotate nearly 50^{o} to accommodate heme binding, and this rotates hydrophobic residues into, and polar residues out of, the aqueous phase(5).

G EIWKQ HEEALKK FEEALKQ FEE-LKKL

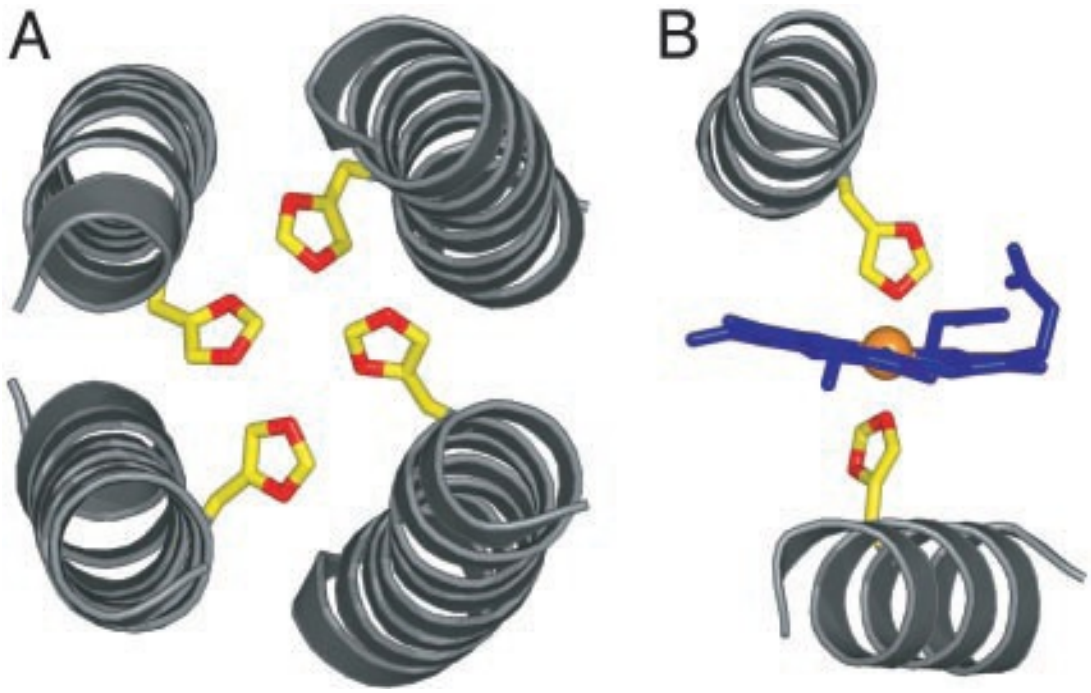

Figure 1.5 Helices bundle rotate while binding heme (Huang, S.L, Koder, R.L. and Dutton, P.L. (2004) *Proc. Nat. Acad. Sci. USA* 101, 5536-41

To enable NMR structure assignment of the backbones, they diversified the amino acids, replacing the repeated c-position E with D, and f-position K with Q. Finally they added a cysteine to the link loop, covalently linking the two proteins with a disulfide bond (5).

G EIWKQ HEDALQK FEEALNQ FED-LKQL GGSGCGSG

G EIWKQ HEDALQK FEEALNQ FED-LKQL

In our project, in addition to HP7, we use two other proteins, HP7H7F and CC9H7F.

HP7H7F:

G EIWKQ FEDALQK FEEALNQ FED-LKQL

GGSGCGSG

G EIWKQ HEDALQK FEEALNQ FED-LKQL

CC9H7F:

G EIWKQ FEDALQK FEEALNQ FED-LKQL

GGSGCGSG

G EIWKQ HADALQK FAEALNQ FAD-LKQL

HP7H7F and CC9H7F differ in their b-position residues. In CC9H7F the charged glutamate is replaced with an uncharged alanine. This glutamate weakens the histidine ligation and allows competition from other ligands. We designed

experiments to check this change and find the strongest heme-binding sites as the first step of designing the p450 (5).

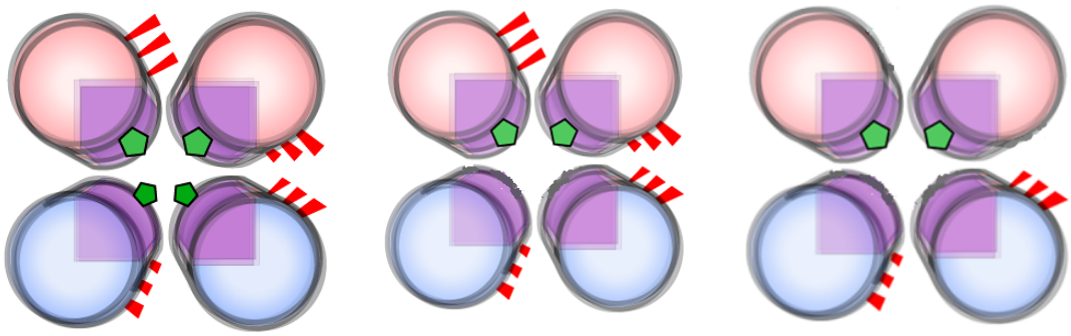

Figure 1.6 The left is HP7H7F with two heme binding sites. The middle is HP7H7F with one heme binding site. The right is CC9H7F, with a single heme binding site, and E replaced with A.

Section 1.3: Ligand Hisitidine Rotamer

Christopher Negron created a database of unique natural heme binding proteins from the PDB. Computational analysis showed that the histidines bound to hemes generally fall into four groups based on their rotamer: t73, t86, m80 and m166 (Figure 7) (12)

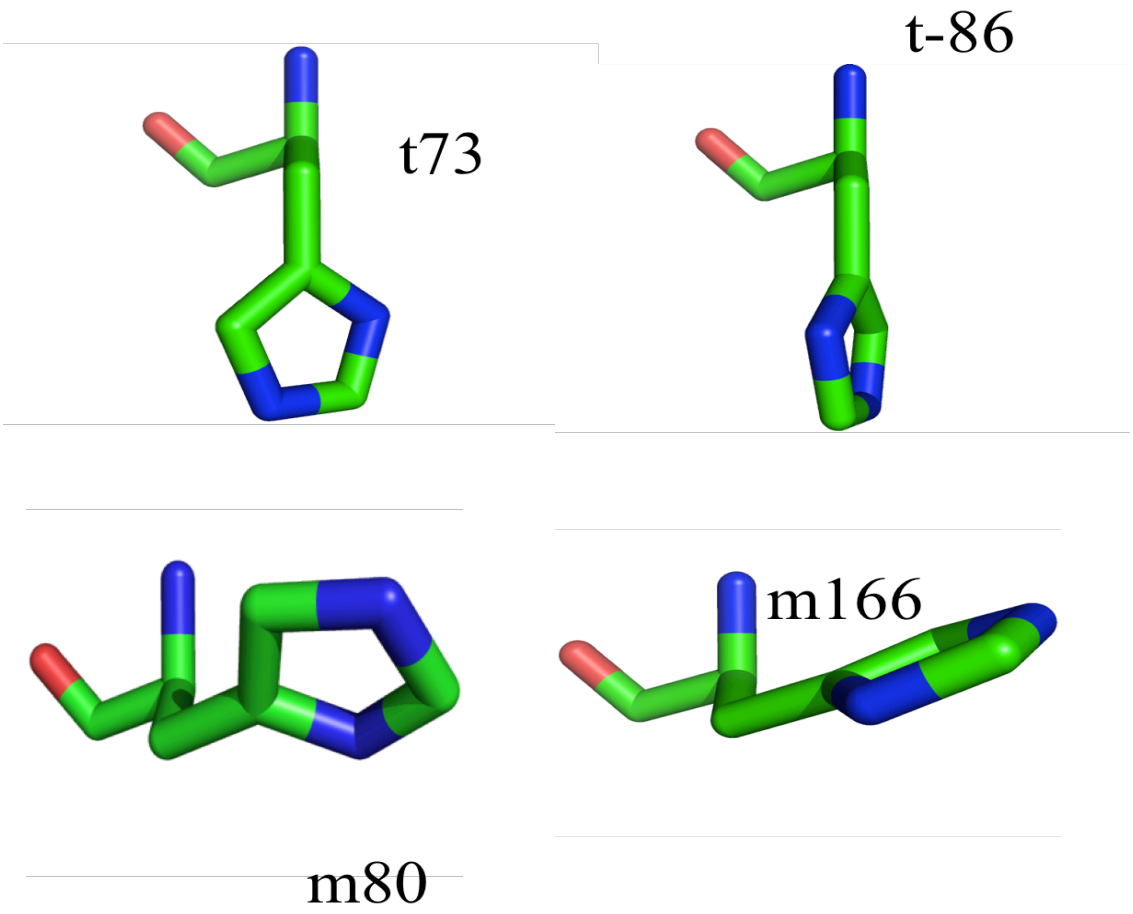

Figure 1.7 Four major histidine rotamers bound to heme. Christopher Negron, Ronald L. Koder(2009)

Analysing each rotamer separately they found prevalent proximal amino acids for each histidine rotamer. (Figure 8-a) Figure 8-b shows frequencies for the subset of histidine-heme binding helices.（12）

Ligand histidine rotamer	Sequence
t73	IIXXXFXXHAXXGIIIF
m166	AXXACXACHXXLA
t-86	AHXXYXXYF
m80	LKXLSXFHXX

C. t73 parallel

	P-8	P-7	P-6	P-5	P-4	P-3	P-2	P-1	P0	P1	P2	P3	P4	P5	P6	P7	P8
ALA	0.0%	6.7%	6.7%	13.3%	6.7%	6.7%	20.0%	6.7%	0%	26.7%	13.3%	13.3%	14.3%	0.0%	8.3%	0.0%	10.0%
ARG	0.0%	0.0%	6.7%	20.0%	0.0%	26.7%	0.0%	0.0%	0%	6.7%	0.0%	6.7%	0.0%	0.0%	16.7%	0.0%	0.0%
ASN	0.0%	0.0%	0.0%	0.0%	0.0%	0.0%	0.0%	0.0%	0%	0.0%	13.3%	6.7%	0.0%	0.0%	0.0%	0.0%	0.0%
ASP	0.0%	0.0%	0.0%	0.0%	0.0%	0.0%	0.0%	0.0%	0%	0.0%	0.0%	0.0%	0.0%	0.0%	0.0%	0.0%	0.0%
CYS	0.0%	0.0%	0.0%	0.0%	6.7%	0.0%	0.0%	0.0%	0%	0.0%	0.0%	0.0%	0.0%	0.0%	0.0%	0.0%	0.0%
GLU	0.0%	0.0%	0.0%	0.0%	0.0%	0.0%	0.0%	0.0%	0%	0.0%	0.0%	0.0%	0.0%	0.0%	0.0%	0.0%	0.0%
GLN	0.0%	0.0%	13.3%	0.0%	0.0%	0.0%	0.0%	0.0%	0%	0.0%	0.0%	0.0%	0.0%	0.0%	0.0%	20.0%	0.0%
GLY	16.7%	20.0%	0.0%	0.0%	6.7%	0.0%	0.0%	0.0%	0%	6.7%	6.7%	13.3%	57.1%	0.0%	8.3%	0.0%	0.0%
HIS	0.0%	0.0%	0.0%	0.0%	0.0%	0.0%	0.0%	0.0%	100%	0.0%	6.7%	0.0%	0.0%	14.3%	0.0%	20.0%	0.0%
ILE	16.7%	33.3%	0.0%	20.0%	20.0%	6.7%	13.3%	20.0%	0%	0.0%	6.7%	6.7%	0.0%	35.7%	33.3%	30.0%	10.0%
LEU	8.3%	13.3%	13.3%	6.7%	6.7%	26.7%	13.3%	20.0%	0%	13.3%	13.3%	6.7%	14.3%	14.3%	0.0%	10.0%	10.0%
LYS	0.0%	0.0%	0.0%	0.0%	0.0%	0.0%	0.0%	0.0%	0%	0.0%	0.0%	6.7%	0.0%	0.0%	0.0%	0.0%	0.0%
MET	8.3%	0.0%	6.7%	13.3%	6.7%	6.7%	13.3%	26.7%	0%	6.7%	6.7%	0.0%	0.0%	7.1%	8.3%	0.0%	20.0%
PHE	8.3%	13.3%	13.3%	13.3%	13.3%	13.3%	6.7%	6.7%	0%	6.7%	6.7%	13.3%	0.0%	14.3%	8.3%	20.0%	30.0%
PRO	0.0%	6.7%	0.0%	0.0%	6.7%	0.0%	0.0%	0.0%	0%	6.7%	0.0%	0.0%	14.3%	0.0%	0.0%	0.0%	0.0%
SER	0.0%	0.0%	0.0%	0.0%	13.3%	0.0%	13.3%	0.0%	0%	0.0%	0.0%	6.7%	0.0%	14.3%	0.0%	0.0%	0.0%
THR	25.0%	0.0%	13.3%	6.7%	0.0%	0.0%	0.0%	0.0%	0%	6.7%	0.0%	0.0%	0.0%	0.0%	0.0%	0.0%	0.0%
TRP	0.0%	0.0%	13.3%	0.0%	0.0%	0.0%	0.0%	0.0%	0%	0.0%	20.0%	6.7%	0.0%	0.0%	8.3%	0.0%	0.0%
TYR	8.3%	0.0%	6.7%	6.7%	6.7%	6.7%	20.0%	13.3%	0%	6.7%	0.0%	0.0%	0.0%	0.0%	8.3%	0.0%	0.0%
VAL	8.3%	6.7%	6.7%	0.0%	6.7%	6.7%	0.0%	6.7%	0%	13.3%	6.7%	13.3%	0.0%	0.0%	0.0%	0.0%	20.0%
Total	12	15	15	15	15	15	15	15	16	15	15	15	14	14	12	10	10

Figure 1.8 Optimal sequences by rotamer (A) and position specific amino acid frequencies for t73 histidine rotamer (B). Christopher Negron, Christian Fufezan, Ronald L. Koder (2009)

Section 1.3: Gaseous Ligand binding Kinetics in Hexacoordinate Hemoglobin

The family of hexacoordinate hemoglobins are oxygen activating enzymes characterized by the property that they are bis-histidine-ligated in the oxidized state and exist in a mixed bis- and mono-histidine ligation state when reduced. (13) The transient pentacoordination of the heme cofactor allows for the binding of molecular oxygen.

Stop-flow techniques and flash photolysis are the traditional and characteristic method to measure the gaseous binding kinetic, such as oxygen, nitric oxide, and carbon monoxide.(15) In order to study the fast reaction kinetic, stop-flow spectroscopic is generally utilized. With the monochromatic light scanning, Two or up to four reagents are mixed together rapidly and stopped in the curvette along with the absorbance changed at specific wavelength, which is record as the function of time.

However, for stop flow mixing, the dead time, which is the time between the end of mixing and the beginning of observation of the reaction kinetic, prevent the measurement during the rapid reaction. Thus the flash photolysis was utilized as the most direct measurement. The protein bond with ligand was applied with lasers or some other light source for long enough time, the protein-ligand bond broke and the ligand was diffused out of the protein binding core. With the laser pulse shut, the rebinding rates can be monitored on the much more rapid time scales than stop flow.

The first step in oxygen activation and/or transport by heme proteins is the binding of molecular oxygen to the ferrous heme iron while avoiding heme oxidation. It is therefore critical to understand the underlying engineering parameters necessary for this process in order to design artificial oxygen utilizing heme proteins. Furthermore, many enzymes which utilize molecular oxygen as a substrate contain a number of redox-active cofactors in addition to the active site heme. Many of these, for example the heme cofactors in the cytochrome c oxidase, serve to transport electrons into the O_2-utilizing heme A-containing active site (*14*). Thus it will further be necessary in the future design of more complex artificial catalysts to be able to restrict ligand binding to those sites where catalysis is intended.

Section 1.4: References

1 Koder,R.L, Dutton,P.L. *et al.* Intelligent design: the de novo engineering of proteins with specified functions *Dalton Trans(2006)*.25:3045-3051

2 Gibney, B.R., and Dutton,P.L(2001) *in Advances in Inorganic Chemistry, Vol 51* pp 409-455

3 Shifman, J.M., Moser, C. C., Kalsbeck, W.A., Bocian, D. F.,and Dutton, P. L. Functionalized de novo designed proteins: Mechanism of proton coupling to oxidation/reduction in heme protein maquettes,(1998) *Biochemistry* 37, 16815-16827.

5 Ronald L.Koder, J.L.Ross Anderson, *et al.* engineering artificial protein function. In press

6. Bernard Meunier, Samuel P. de Visser and Sason Shaik. Mechanism of Oxidation Reactions Catalyzed by Cytochrome P450 Enzymes *Chem. Rev.* **2004,** *104,* 3947-3980

7. Ho, S. P., and Degrado, W.F. Design of a 4-helix bundle protein-Synththesis of Peptides Which Self-Associste into a Helical Protein,(1987) *Journal of the American Chemical Society* 109, 6751-6758

8. Lear,J.D., Wasserman,Z.R., and Degrado, W.F. Synthetic Amphiphilic Peptide Models for Protein Ion Channels, (1988) *Science 240*, 976-978

9. Degrado,W.F., Wasserman,Z.R,and Lear,J.D. Protein design, a Minimalist Approach, (1989) *Science 243*, 622-628

10. Mathias A.S.Hass, Lewis E. Kay. *et al.* Characterization of Conformational Exchange of a Histidine Side Chain:Protonation, Rotamerization, and Tautomerization of His61 in Plastocyanin from Anabaena variables. *J.Am.CHEM.SOC*

11. Koder,R.L, Dutton,P.L Nativelike Structure in designed Four α-helix Bundles Driven by Buried Polar interactions (2006)J.AM.CHEM.SOC.128:14450-14451

12. Negron, C., Fufezon, C., Koder, R.L. Geometric Constraints for Porphyrin Binding in Helical Protein Binding Sites (2008) *Proteins: Struct. Func. Bioinf*

13. Brunori, M., Giuffre, A., and Sarti, P. (2005) Cytochrome c oxidase, ligands and electrons, *Journal Of Inorganic Biochemistry 99*, 324-336.

14. Trent, J. T., Hvitved, A. N., and Hargrove, M. S. (2001) A model for ligand binding to hexacoordinate hemoglobins, *Biochemistry 40*, 6155-6163

15. Olson J.S. Stopped-flow, rapid mixing measurements of ligand binding to hemoglobin and red cells (1981) *Methods in Enzymology*, 76 (C), pp. 631-651

Chapter 2: Manipulating Binding Thermodynamics in an Artificial Neuroglobin

Section 2.1: Summary

HP-7 is one artificial mutated oxygen transport protein, which operates via a mechanism akin to human neuroglobin and cytoglobin. This protein destabilizes one of two heme- ligating histidine residues by coupling histidine side chain ligation with the burial of three charged glutamate residues on the same helix. Replacement of these glutamate residues with alanine, which has a neutral hydrophobicity, slows gaseous ligand binding 22-fold, increases the affinity of the distal histidine ligand by a factor of thirteen, and decreases the binding affinity of carbon monoxide, a nonreactive oxygen analogue, three-fold. Paradoxically, it also decreases heme binding affinity by a factor of three in the reduced state and six in the oxidized state. Application of a two-state binding model, in which an initial pentacoordinate binding event is followed by a protein conformational change to hexacoordinate, provides insight into the mechanism of this seemingly counterintuitive result: the initial pentacoordinate encounter complex is significantly destabilized by the loss of the glutamate side chains, and the increased affinity for the distal histidine only partially compensates. These results point to the importance of considering each oxidation and conformational state in the design of functional artificial proteins.

Section 2.2: Introduction

Designed proteins containing bound cofactors, both natural and synthetic, hold great promise as inexpensive biocompatible catalysts useful in medicine, energy production and green industrial catalysis (*1-3*). Heme proteins were the first bioinorganic-cofactor containing proteins created over fifteen years ago (*4, 5*), and since then they have proven instructive as to the underlying engineering requirements which drive natural heme protein evolution (*6-8*). The family of hexacoordinate hemoglobins are characterized by the property that they are bishistidine-ligated in the oxidized state and exist in a mixed bis- and mono-histidine ligation state when reduced (*9*). The transient pentacoordination of the heme cofactor allows for the ligation of molecular oxygen. We have recently reported the design, bacterial expression, and biochemical analysis of the completely artificial hexacoordinate oxygen transport protein HP7(*10*). This was the culmination of a series of design projects involving helical bundles which bind heme (*11-16*). The homodimeric protein HP7 is composed of two helix-loop-helix peptides in which the loops connect via a disulfide in a topology we have termed the 'candelabra' motif(*12*) (see Figure 1A, sequences in 1E).

HP7 and its progenitors were designed in part using the principles of binary patterning, a simple alternating pattern of hydrophilic and hydrophobic helix-forming residues with the heptamer repeat sequence ●○○●●○○, where the first, third and fourth amino acids are non-polar (●) and the rest polar (○)(see Figure 1E) which imposes dimerization via hydrophobic sequestration (*17-21*). Each residue in the

heptad repeat is designated with a letter, thus the hydrophobic residues are at the a, d and e positions of the heptad. There is a histidine residue at the sixth position of each helix, positioned to lie at the aposition of the heptad repeat (*13*). Two heme cofactors bind, one between each matching pair of histidines in the homodimer, and each binding event induces a large-scale helical rotation which brings three b position glutamate residues into the hydrophobic core of the protein. The burial of these residues creates an 'entatic' state (*22*): this stored energy is utilized to drive the detachment of the ligand histidine residue on that helix enabling the subsequent rotation of the helix to a relaxed state in which these bposition side chains are exposed to solvent, opening a coordination site for the ligation of the gaseous ligands oxygen and carbon monoxide (Figure 1B-D) (*10*). This design exercise turned out to be instructive as to the minimal engineering requirements for oxygen transport – a porphyrin cofactor with at least a transiently pentacoordinate ferrous iron buried within a hydrophobic cavity sufficiently large and stable as to restrict water penetration (*11*).

Thus in HP-7 as well as the natural hexacoordinate hemoglobins gaseous ligand affinity is gated by the presence of the pentacoordinate state. Many enzymes, especially those which utilize molecular oxygen as a substrate, contain a number of redox active cofactors in addition to the active site heme. These other cofactors, for example the heme cofactors in the cytochrome c oxidase, typically serve to ferry electrons into the O2-utilizing active site (*23*). These enzymes restrict oxygen binding at the other heme cofactors by maintaining them in the hexacoordinate state.

Therefore it will prove important, in the future design of more complex artificial catalysts, to be able to effectively create high affinity cofactor binding sites with controllable distal ligand affinity. It is therefore important to understand the factors which determine distal side chain affinity and its relationship to overall cofactor binding affinity.

Section 2.3:Materials and Methods

Chemicals. Oligonucleotides were purchased from Integrated DNA Technologies (Coralville, IA) and used without further purification. ^{15}N-labelled ammonium chloride was purchased from Cambridge Isotope Labs (Cambridge, MA). Pyocyanine was purchased from Cayman Chemical (Ann Arbor, MI). Hemin was purchased from Fluka (Buchs, Switzerland). All other solvents and reagents were from either Fisher Scientific or Sigma.

Cloning, protein expression and purification. The CC9 gene was synthesized (Biomatik Corp., Cambridge, ON) with an N-terminal TEV cut site and inserted between the BamHI and XhoI restriction sites of pET32a (+) (Novagen) as previously described (*12*). Mutagenesis to produce CC9-H7F and HP7-H7F was accomplished using the Quikchange method (Stratagene Inc., La Jolla, CA). Mutagenized plasmid DNA was transformed into chemically competent DH5α *E. coli*, the resulting clones verified by sequencing, and a verified plasmid was transformed into BL21(DE3) cells for expression.

For unlabelled expression, cells were grown in TPP medium at 37° C to an OD_{600} of 1.0 and induced with 0.5 mM IPTG at 25° C for 5 h before collection. For ^{15}N-labelled expression, cells were grown at 37° C in M9 minimal media containing 1 g/L ^{15}N ammonium chloride to a OD_{600} of 1.0, induced with 1 mM IPTG, and shaken at 25° C for an additional 7 h. Both HP7-H7F and CC9-H7F were expressed as his_6-tagged thioredoxin fusion proteins, cleaved with tobacco etch virus protease

and purified using nickel chromatography as reported for HP7 (*12*). Apoprotein solutions were then dialyzed into 250 mM Boric Acid, 100mM KCl, pH 9.0 overnight to ensure homodimer disulfide formation. Apoprotein concentrations were determined optically using ε_{280} = 11.5 $mM^{-1}cm^{-1}$ on the basis of their tryptophan content (*24*).

Holoprotein complexes, containing 1.0 equivalent per homodimer, were prepared as before (*12*) by five consecutive additions of 0.2 equivalents of hemin in DMSO with at least ten minutes between additions. Proteins were then purified from any unbound heme by passage through a PD10 desalting columns pre-equilibrated with 250mM Boric Acid, 100mM KCl pH 9.0. Holoprotein solution concentrations were determined using experimentally derived Soret ε_{414} = 129 $mM^{-1}cm^{-1}$ for HP7-H7F and 118 $mM^{-1}cm^{-1}$ for CC9-H7F. If necessary, both holo- and apoproteins were concentrated using Centricon YM-10 spin concentrators (Millipore, Inc., Billerica, MA).

General biochemistry. Optical spectra were collected with a Hewlett-Packard (New York, NY) 8452A Diode array spectrophotometer equipped with a Quantum Northwest (Liberty Lake, WA) Peltier temperature controller. Experiments requiring anaerobic conditions were conducted in an anaerobic cuvette (*25*) equipped with a platinum working and Red Rod (Radiometer Analytical, Lyon, France) reference electrode. All experiments were performed at 20° C in 250mM Boric Acid, 100mM KCl pH 9.0 unless otherwise noted. Each binding, reduction potential and

stopped flow experiment was performed at least three times and reported errors are standard deviations from the mean.

Circular dichroism spectropolarimetry. CD spectra were recorded on a JASCO J-810 sepectropolarimeter in a quartz cell of 0.1cm light-path, using a bandwidth of 1nm and a scan speed of 50nm/min. HP7-H7F and CC9-H7F were prepared at concentrations of 24.15μM and 14.75μM respectively in 50mM sodium phosphate, pH 7.5. Spectra were collected between 190nm and 280nm, with background correction. The spectra were observed as ellipticity (θ_{obs}, mdeg), and the mean residue ellipticity([θ],deg•cm2•dmol-1) were calculated as

(1) $[\theta]=[\theta]_{obs}\bullet$ [MRW/(*10lc*)]

Where MRW is the mean residue molecular weight, *c* is the sample concentration in mg/ml, and *l* is the light-path length of the cell in cm. Protein secondary structure percentages were calculated with the program K2d (*26*) using data points ranging from 200nm to 240nm.

Stopped Flow analysis of CO binding and distal histidine dissociation. Binding kinetics of CO with the ferrous protein-heme complexes were followed spectroscopically in rapid stopped-flow mixing experiments over gas concentrations from 2% to 50% saturation at 15° C using an Olis RSM 1000 spectrometer that scans both the alpha band and Soret band absorptions 1,000 times a second followed by SVD analysis of the kinetic components. Protein concentrations were 20-25 μM and

ferrous complexes were prepared by carefully titrating anaerobic solutions of the holoproteins with a slight excess of dithionite as observed by visible spectroscopy. Ferrous samples were anaerobically transferred to the stopped-flow loading syringe by canula. Binding kinetic data were fit with Eqn. 2, which assumes that CO binding rate, k_{+CO} , is much greater than the sum of the distal histidine association and dissociation rates (*9*):

$$(2)\quad k_{obs} = \frac{k_{-H} k_{+CO}[CO]}{k_{+H} + k_{-H} + k_{+CO}[CO]}$$

Where k_{obs} is the fitted single exponential binding rate, k_{+H} and k_{-H} are the distal histidine-ferrous heme iron association and dissociation rates and k_{+CO} is the CO association rate constant. At high [CO]. $k_{obs} = k_{-H}$.

Flash photolysis analysis of distal histidine association. The rate constants for both CO and histidine binding to the pentacoordinate state were determined using laser flash photolysis: a 1-ns pulse-width frequency doubled YAG laser at 532 nm excites the preformed carbonmonoxyferrous complex, causing the detachment of the ligand CO. This transiently forms an unliganded pentacoordinate heme protein and the rates of these binding processes were determined by analyzing the multi-exponential rebinding traces taken as a function of CO concentration using the method of Hargrove (*27*):

$$(3)\ \gamma_1 + \gamma_2 = k_{-H} + k_{+H} + k_{+CO}[CO]$$

(4) $\gamma_1\gamma_2 = k_{-H}k_{+CO}[CO]$

Where γ_1 and γ_2 are the fitted first and second CO-dependent exponential rates and the kinetic constants are defined as in Equation 2. Protein concentrations were 20-25 μM and carbonmonoxyferrous complexes were prepared by titrating solutions of the holoproteins with an excess of dithionite as observed by visible spectroscopy under an atmosphere containing 10-100% CO mixed with argon.

Heme affinity measurements. Hemin stock solutions of approximately 0.5-1.0 mg/ml were prepared in DMSO and used within six hours. Stock solution concentrations were determined using the pyridine hemochrome assay (*28*). In oxidized binding experiments 0.5-2 μl aliquots of hemin solution, consisting of approximately 0.1 molar equivalents, were added via gastight syringe to a stirring 4 ml solution of 2-3 μM protein, with a ten minute equilibration delay between additions. Heme binding was monitored by loss of the absorption at 385 nm due to free hemin, and the concomitant appearance of a sharp Soret band at 412 nm, corresponding to heme bound to the protein via bis-histidine axial coordination. The number of heme binding sites was quantified for each protein from plots of the Soret maximum at 412 nm *vs* the number of equivalents added.

For reduced binding experiments, 9.0 ml of ~3 μM protein was made anaerobic by extended flushing with nitrogen, and the solution potential reduced to < -450 mV vs NHE by the addition of a small volume (< 20 μl) of sodium dithionite

dissolved in degassed 100 mM KOH. The solution potential was monitored throughout the binding titration and kept below -450 mV by periodic additions of µl volumes of sodium dithionite. Hemin was added in approximately 0.1 molar equivalent aliquots with at least a ten minute equilibration time before spectra were collected. K_d values were obtained from plots of the Soret band absorbance measured at 436 nm vs. the concentration of hemin added and fit with the tight binding equation:

(5)

$$\Delta A = A_{start} + \varepsilon_{unb}[hem] + \varepsilon_{bnd}[prot] \cdot \left[\frac{K_d+[hem]+[prot]-\sqrt{(K_d+[hem]+[prot])^2-4[hem][prot]}}{2[prot]}\right]$$

Where ε_{unb} is the molar absorption coefficient of unbound hemin at that wavelength, ε_{bnd} is the additional absorbance of bound hemin at that wavelength, [hem] is the hemin concentration, [prot] is the protein concentration and K_d is the dissociation constant for the reduced hemin.

Reduction potential determination. Redox titrations were performed in combination with optical analysis as described previously (*13*). Concentrated solutions of hemoprotein prepared in advance were diluted to 20-30 μM into a solution containing >100 µM of the corresponding apoprotein in order to eliminate the possibility of heme dissociation upon reduction (*28*). Reported reduction potentials are referenced to a standard hydrogen electrode. All redox titrations were performed anaerobically using μL additions of freshly prepared sodium dithionite to adjust the

solution potential to more negative values and potassium ferricyanide to more positive values. The following redox mediators were used to stabilize solution redox potential: 25 μM 2,3,5,6-tetramethylphenylenediamine, 25 μM 1,2-naphthoquinone, 20 μM phenazine methosulfate, 20 μM phenazine ethosulfate, 50 μM duroquinone, 10 μM pyocyanine, 6 μM indigo trisulfonate, 25 μM 2-hydroxy-1,4-naphthoquinone, 20 μM phenazine, 20 μM anthroquinone-2-sulfonate, 20 μM benzyl viologen and 20 μM methyl viologen. Redox titrations were analyzed by monitoring the absorbance bands at 559 and 425 nm as the heme protein was reduced or oxidized. The data were analyzed with the Nernst equation using an *n*-value of 1.0:

(6) $$\%\boldsymbol{R} = \frac{\mathbf{1}}{\mathbf{10}^{(\boldsymbol{E}-\boldsymbol{E_m})/[(\frac{\boldsymbol{RT}}{\boldsymbol{nF}})]}}$$

where %R is the fraction of reduced heme, E is the solution potential, E_m is the reduction midpoint potential and n is the number of electrons.

Nuclear magnetic resonance. All NMR experiments were performed at 20^{o}C on Varian Inova spectrometer operating at a 600MHz and equipped with a triple resonance cryogenic probe capable of applying pulse field gradients in the z-direction. Data were processed using the program NMRPipe (*29*) and analyzed using Sparky (*30*). For structural specificity assays, sensitivity enhanced ^{1}H-^{15}N heteronuclear single quantum coherence (HSQC) spectra (*31*) were collected on 50-100 μM holo- and apoprotein samples with sweep widths of 10,000 Hz for ^{1}H and 2000 Hz for ^{15}N utilizing GARP decoupling of ^{15}N during ^{1}H acquisition. Chemical shifts are referenced to water at 4.77 ppm for ^{1}H.

In order to determine the pK_a of histidine side chains, imidazole ^{1}H-^{15}N multiple-bond correlation signals were collected using a non-sensitivity enhanced HSQC pulse sequence in which the INEPT (insensitive nuclei enhanced by polarization transfer) periods were set to $1/^{1}J_{NH}$, where $^{1}J_{NH}$ is the one-bond ^{1}H-^{15}N coupling constant, in order to attenuate backbone amide signals (*32, 33*). Spectral widths were 8000 Hz for ^{1}H and 12156 Hz for ^{15}N. Lyophilized ^{15}N-labelled apoprotein samples were dissolved in 25mM KaD_2PO_4 D_2O buffer pD 5.0 (pH meter reading + 0.4 pH units), a spectrum taken, and the pD adjusted upwards by the addition of small amounts of KOD dissolved in D_2O. The observed ^{15}N chemical shifts were fit with the Henderson-Hasselbach equation:

$$(7)\quad \delta_{obs} = \frac{\Delta\delta_{prot}}{1+10^{[pH-pKa]}} + \delta_0$$

where δ_0 is the neutral chemical shift of ^{15}N, δ_{prot} is the change in chemical shift due to protonation and pK_a is the fitted acid dissociation constant.

Section 2.4:Results and Discussion

Protein design. To simplify our analysis, we removed one binding site by mutating the histidine on the first helix to a phenylalanine, creating the protein HP7-H7F (see Table 1). This protein retains the heme binding site nearest the connecting loops (Figure 1A). To examine the thermodynamic effects of the buried charges, all three b-position glutamates on the second helix were mutated to alanine, which has both neutral hydrophobicity and high helical propensity (*34*).

Both holoproteins display visible absorbance spectra indicative of bis-histidine coordination in both oxidation states (Figure 2A & C). It is important to confirm the helical bundle structure of each protein, as some designed helical bundle proteins have been found to form domain-swapped higher oligomeric states (*35*). Both apo- and holoprotein forms of both HP7-H7F and CC9-H7F were single homodimers as analyzed by native gel electrophoresis in both the holo- and apostates (data not shown). Circular dichroism spectra on the apo forms of both proteins demonstrate that both proteins are helical, with CC9-H7F having a larger helical character. Thisis unsurprising in that each homodimer contains six mutations from glutamic acid to alanine, which has a significantly higher helical propensity (*36*). Both had 15N-HSQC spectra indicative of molten globular structure (not shown). The addition of a single heme cofactor changes both spectra to a level of chemical shift dispersion indicative of a partial phase transition in which the two helices which ligate the heme become native-like and the two unliganded helices remain molten globular, consistent with what we have previously observed for HP7 (*12*).

Oxidized heme binding. In the oxidized state, both proteins bind heme too tightly to reliably extract a dissociation constant even at protein concentrations as low as 200 nM. This has enabled us to perform endpoint titrations confirming that both proteins bind a single heme cofactor (Figure 2) as well as calculate the extinction coefficient of the oxidized complex (Table1).

Table 2.1 Characterization of the two HP7 variants

	$\lambda_{max\_Oxidized}$ ($mM^{-1}cm^{-1}$)	$\lambda_{max\_Reduced}$ ($mM^{-1}cm^{-1}$)	$\lambda([\theta]_{222}$ (deg cm^2 $dmol^{-1}$)	% α-helix
HP7H7F	414(129) 530(12.8) 558(10.1)	428(140) 532(12.1) 560(20.9)	222(-8307)	42
CC9H7F	414(118) 530(11.1) 556(9.1)	426(139) 530(12.6) 560(22.0)	222(-15925)	59

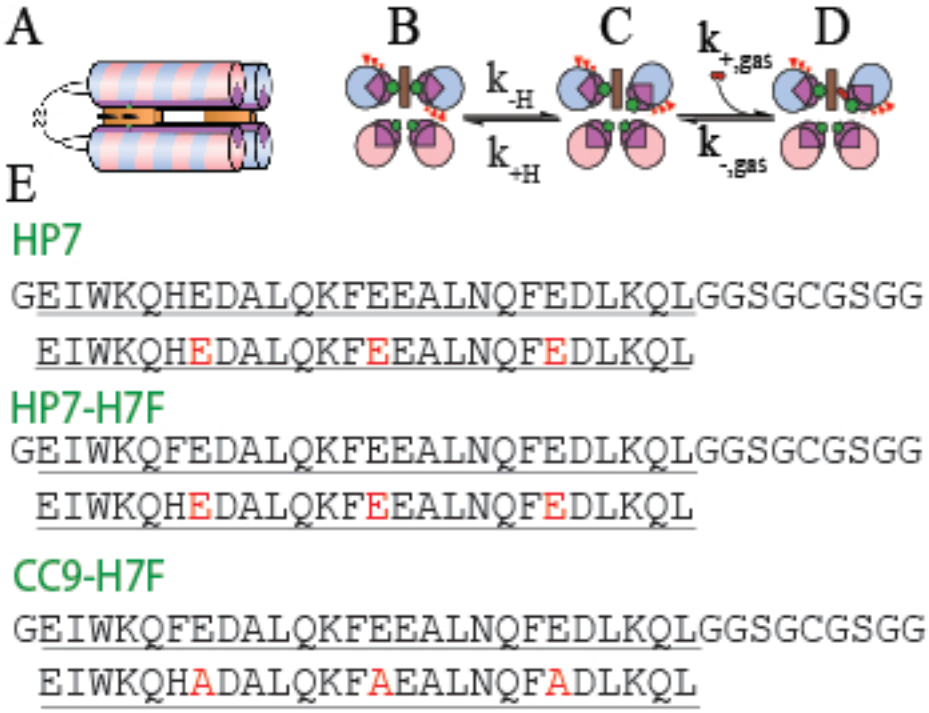

Figure 2.1 Structure, sequence and mechanism of HP7 and its mutants. (A) All three proteins are homodimers in a candelabra configuration in which the helix-loop-helix monomers are connected by a disulfide bond in the loop region. (B-D) Mechanism of gaseous ligand biding. State (B) is the entatic state. (E) Sequences of HP7, the distal heme binding site knockout mutant HP7-H7F, and the entatic state stabilizing mutant CC9-H7F. Helices are underlined and the b-position residues mutated in the transition from HP7 to CC9 are in red.

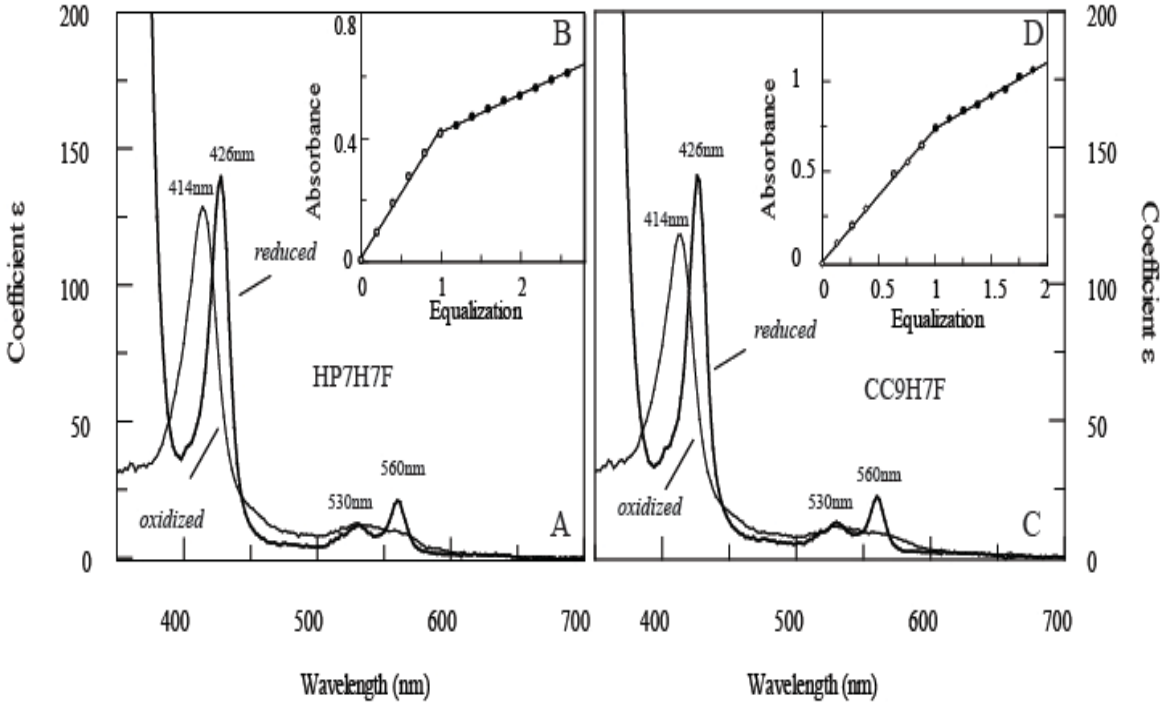

Figure 2.2 Absorption spectra and oxidized binding titrations of HP7-H7F and CC9-H7F with oxidized heme. (A) Oxidized and reduced spectra of heme-bound HP7-H7F. Extinction coefficients are calculated using the intercepts from the endpoint titrations in (B). (C) Oxidized and reduced spectra of heme-bound CC9-H7F, calculated using the data from (D).

Distal histidine affinity --- histidine dissociation constant. In order to confirm that the triple mutation indeed stabilizes the affinity of the distal histidine, we must separately determine its association and dissociation rates. Figure 3 depicts the observed CO binding constants and their concentration dependence. For both proteins, CO binding to the ferrous state is monoexponential over more than five half-lives. Binding rates collected as a function of CO concentration demonstrate that CC9-H7F binds CO 22-fold more slowly than HP7-H7F (Table2). As the protein is primarily in the hexacoordinate bis-histidine ligation state in solution, the rate limiting step for CO binding at high ligand concentrations is thus the detachment of the distal histidine from the heme iron (see Eqn. 2). Thus, histidine detachment is also 22-fold slower in CC9-H7F.

Distal histidine affinity --- CO-flash photolysis determination of k+His. Figure 4 depicts the rebinding kinetics of CO after laser induced dissociation in CC9-H7F. In CC9-H7F, HP7-H7F, and our original analysis of HP7 (*10*), a fast exponential process which is independent of the concentration of CO is observed. Similar behavior has been observed in mouse neuroglobin, and was ascribed to a relaxation process following a probable rearrangement caused by the change in heme iron planarity induced by detachment of the CO ligand (*37, 38*). In each case two slower exponential processes, each of which varies in rate and magnitude with CO concentration, were also observed.

Replots of the sums and products of these two exponential processes are depicted in Figure 5. The distal histidine binding rates are similar in both proteins, with the triple mutation slowing this process by a factor of 1.7 (Table 2). Combining these rates with the histidine off-rates determined in the stopped flow experiments allows the calculation of the distal histidine affinity constants, KA, for both proteins – 30 for HP7-H7F increasing to 380 for CC9-H7F (as this is an intramolecular interaction, the association constant is dimensionless). Thus the removal of the residues which were implanted to create the entatic state in HP7 stabilizes the hexacoordinate state in the ferrous protein by 1.5 kcal/mol.

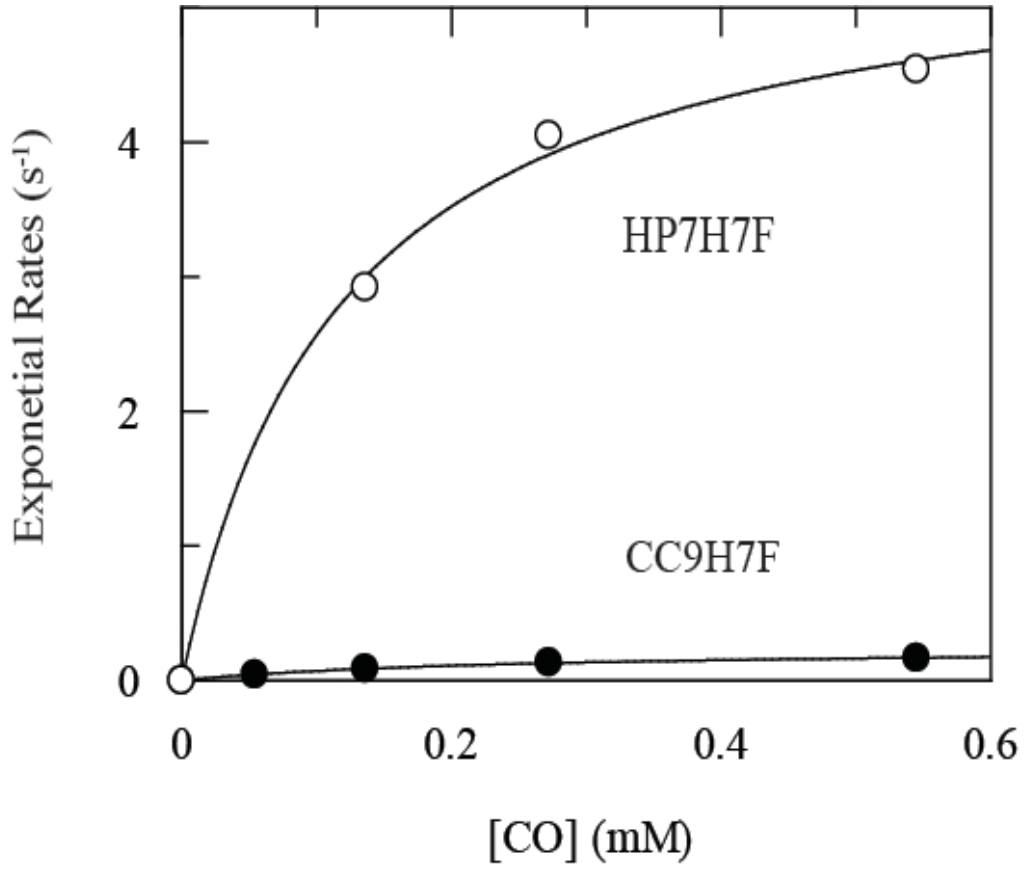

Figure 2.3 Kinetic analysis of CO and histidine binding to HP7-H7F and CC9-H7F. Stopped-flow analysis of the rates of CO binding to reduced heme proteins as a function of ligand concentration. Lines are fits with eqn. 2.

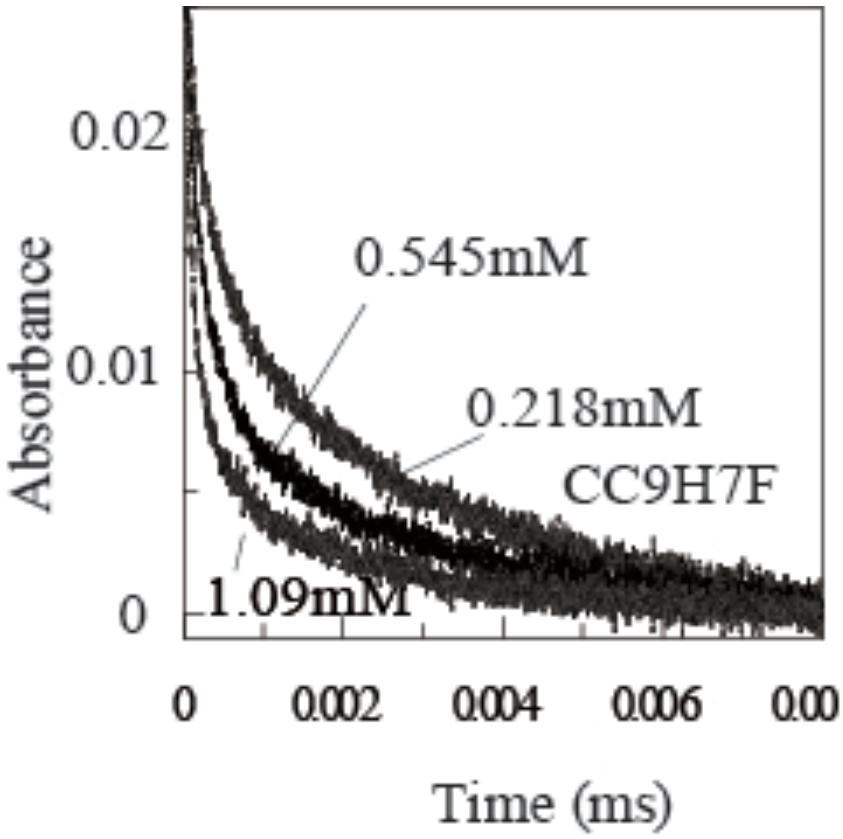

Figure 2.4 Laser flash kinetic analysis of histidine and CO rebinding to CC9-H7F followed at 419 nm. These data were fit with three exponentials, the first of which represents a [CO]-independent relaxation process.

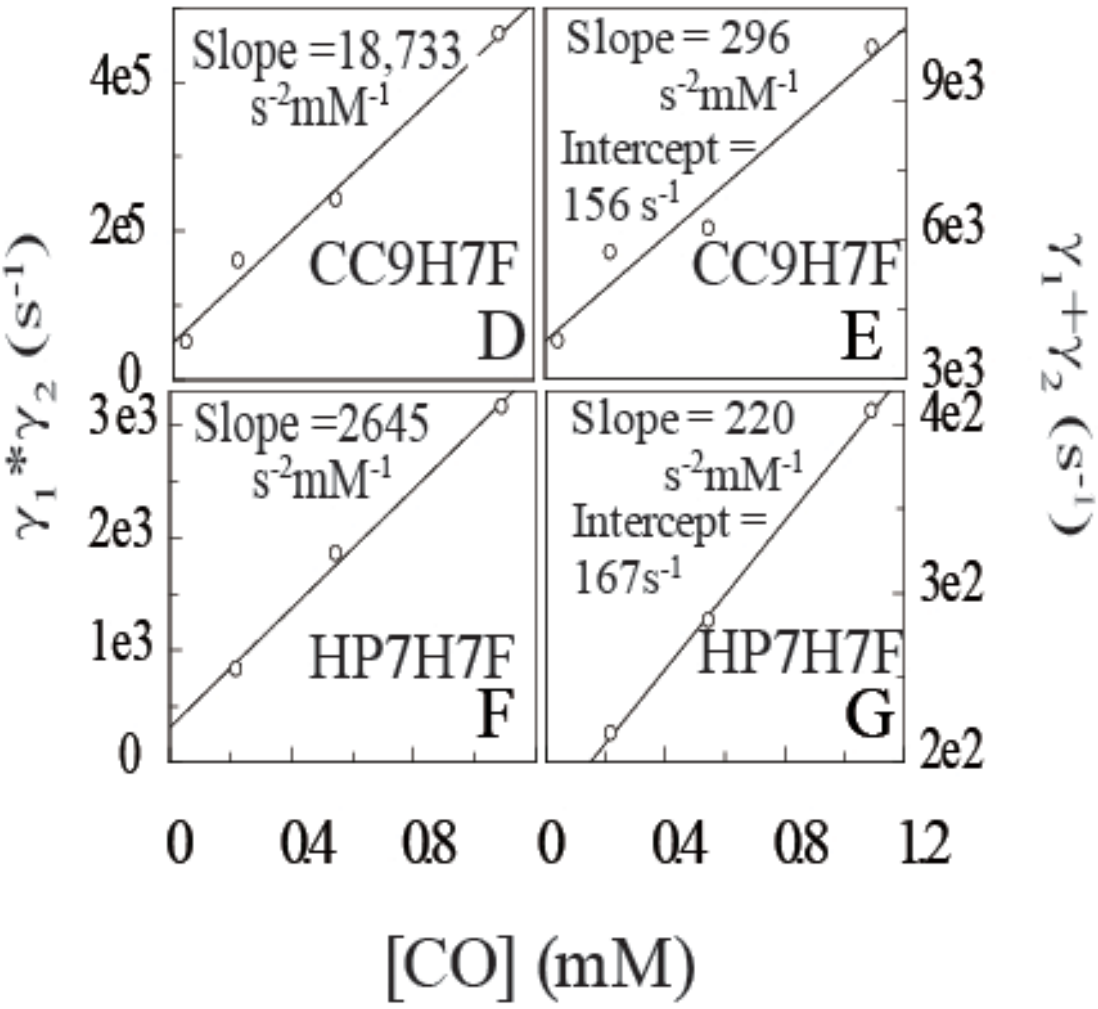

Figure 2.5 (C) Laser flash kinetic analysis of histidine and CO rebinding to CC9-H7F and HP7H7F heme ferrous complex followed at 419 nm. Replots of the sums and products of the second two exponentials.

Heme binding. Gibney and coworkers have determined the solution reduction potential of an isolated heme cofactor, -63 mV vs SHE, using two different designed heme proteins and a thermodynamic cycle (*39*). This value enables an alternate method for the determination of heme binding constants: experimentally determine the binding affinity in the reduced state, taking advantage of the weaker histidine-ferrous heme iron interaction (*40*), then the oxidized heme binding constant can be calculated in combination with the bound and unbound heme reduction potentials using a similar thermodynamic cycle (see Figure 6). Binding titrations carried out under reducing conditions give reproducible binding curves (see Figure 7A,C) and the fitted ferrous heme dissociation constants were 0.6 ± 0.2 μM for HP7-H7F and 2.6 ± 0.6 μM for CC9-H7F.

Reduction potentials. The potentiometric analysis of the two proteins is depicted in Figure 8. HP7-H7F, at -260 ± 6 mV vs NHE, has a reduction potential 65 mV lower than CC9-H7F (see Table 2). As HP7 complexed with two hemes has a reduction potential of -300 mV vs NHE (*10*), each set of three buried glutamates imparts a change in reduction potential of approximately -50 mV, or 1.2 kcal/mol. This, coupled with the reduced affinities, allows the calculation of oxidized affinities of 3 ± 1 nM and 19 ± 3 nM for HP7-H7F and CC9-H7F respectively. These potentials also provide an explanation for the observed differences in oxidation rates during the ferricyanide trapping experiments – electron transfer is 1.2 kcal/mol more favorable from the lower potential heme complex in HP7-H7F.

The weaker affinity for heme binding in the case of CC9-H7F, which has already been shown to bind the distal histidine with a twelve-fold higher affinity in the ferrous state, is counterintuitive. This discrepancy might be explained by a large difference in bound cofactor reduction potentials, caused by some alteration in the local structure and/or electrostatics that moves the heme potential in the negative direction. The potentials, however, move in the direction predicted by simple electrostatics (positive), and thus the ferric heme binding energy difference between CC9-H7F and HP7-H7F is even larger.

Table 2.2 | Thermodynamic for two artificial haem protein

Haem Protein	$K^{*}_{d\text{-}red}$ (μM)	$E^{\dagger}_{mid}$ (mV)	$K^{\ddagger}_{d\text{-}ox}$ (nM)	pKa¶	K+his (s^{-1})	k-his (s^{-1})	$K_{A,his}$§	K_{d_pen}‖ (μM)
HP7H7F	0.6±0.2	-260±6	0.3±0.1	7.3±0.2	160±20	5.6±0.3	29±5	18±9
CC9H7F	2.9±0.4	-195±2	19±3	6.39±0.01	94±11	0.25±0.01	380±60	1100±300

* hexa-coordinates dissociation rates in reduced stated

† middle reduction potential.

‡ dissociation rates in oxidized state by calculating thermodynamic box.

¶ logarithmic measure of the acid dissociation constant

§ association constant for the second histine bound the heme

‖ penta-coordinates dissociation rates in reduced state

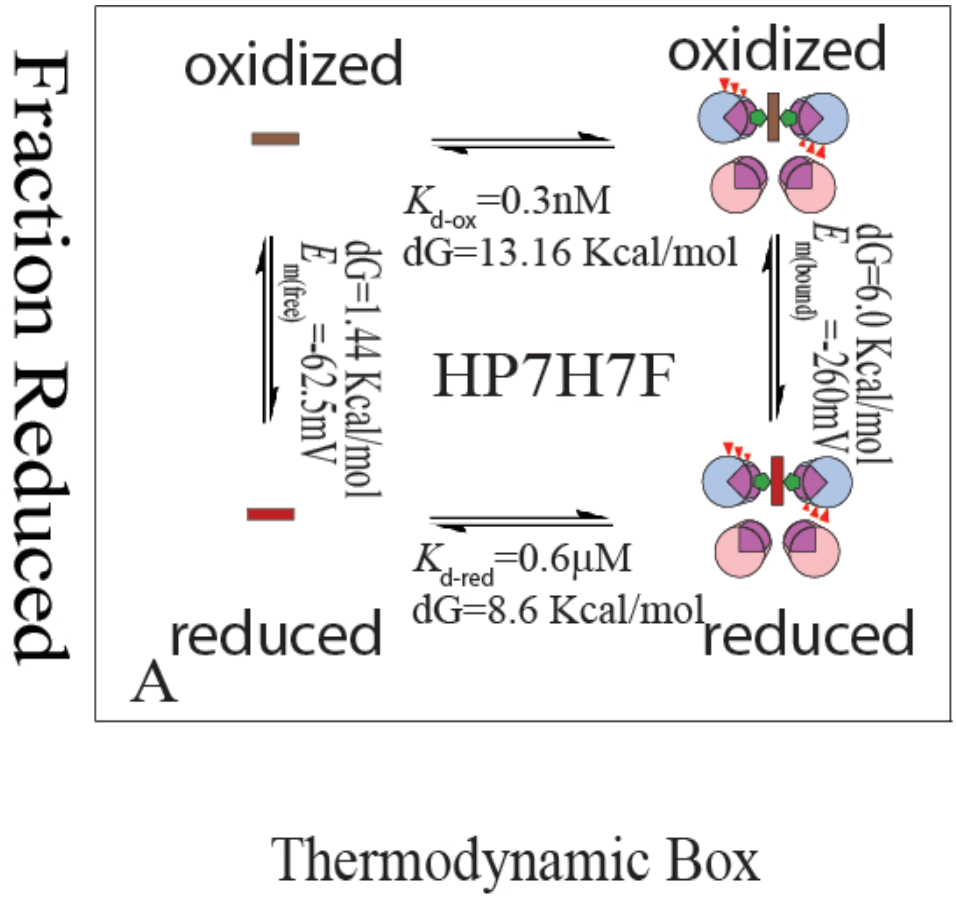

Figure 2.6 The thermodynamic box used to determine $K_{d,ox}$.

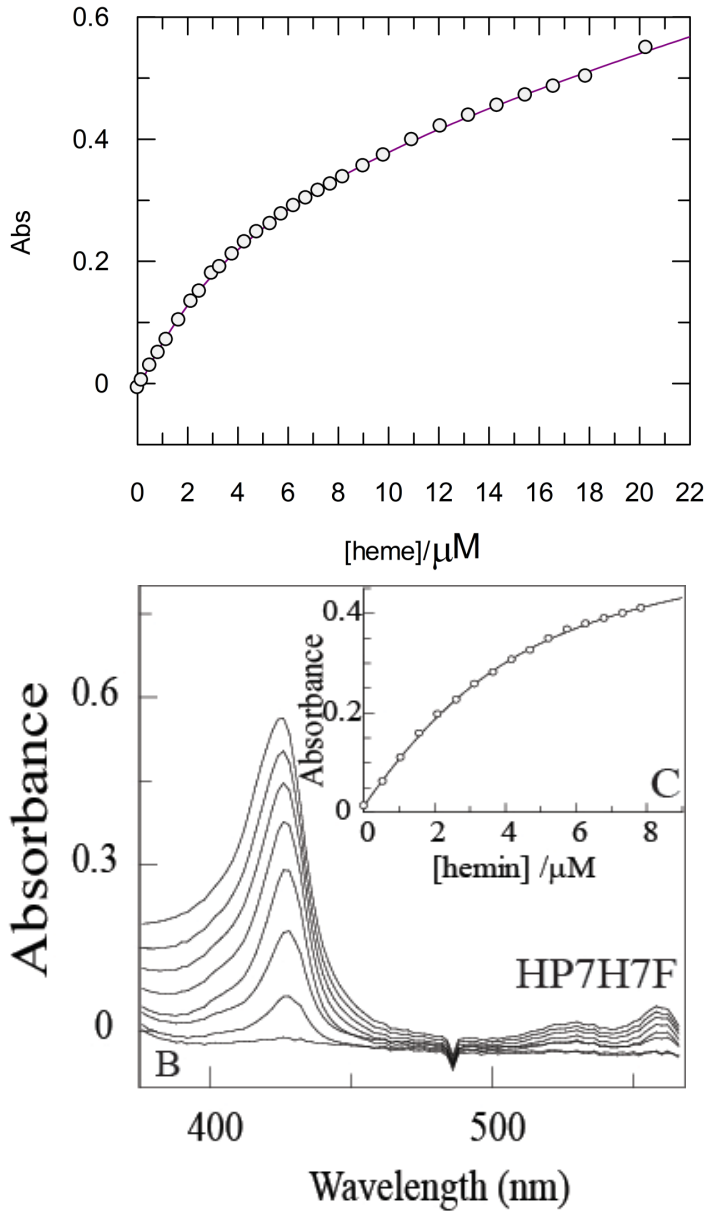

Figure 2.7 (A) Equilibrium binding isotherm derived from the titration. The line drawn is a fit with Eqn. 5 using a Kd,red of 2.6 μM (B) Spectrometric titration of reduced heme binding to 3.0 μM HP7-H7F in 250mM Boric Acid, 100mM KCl pH 9.0. Some spectra have been omitted for clarity. (C) Equilibrium binding isotherm derived from the titration in (B). The line drawn is a fit with Eqn. 5 using a $K_{d,red}$ of 600 nM.

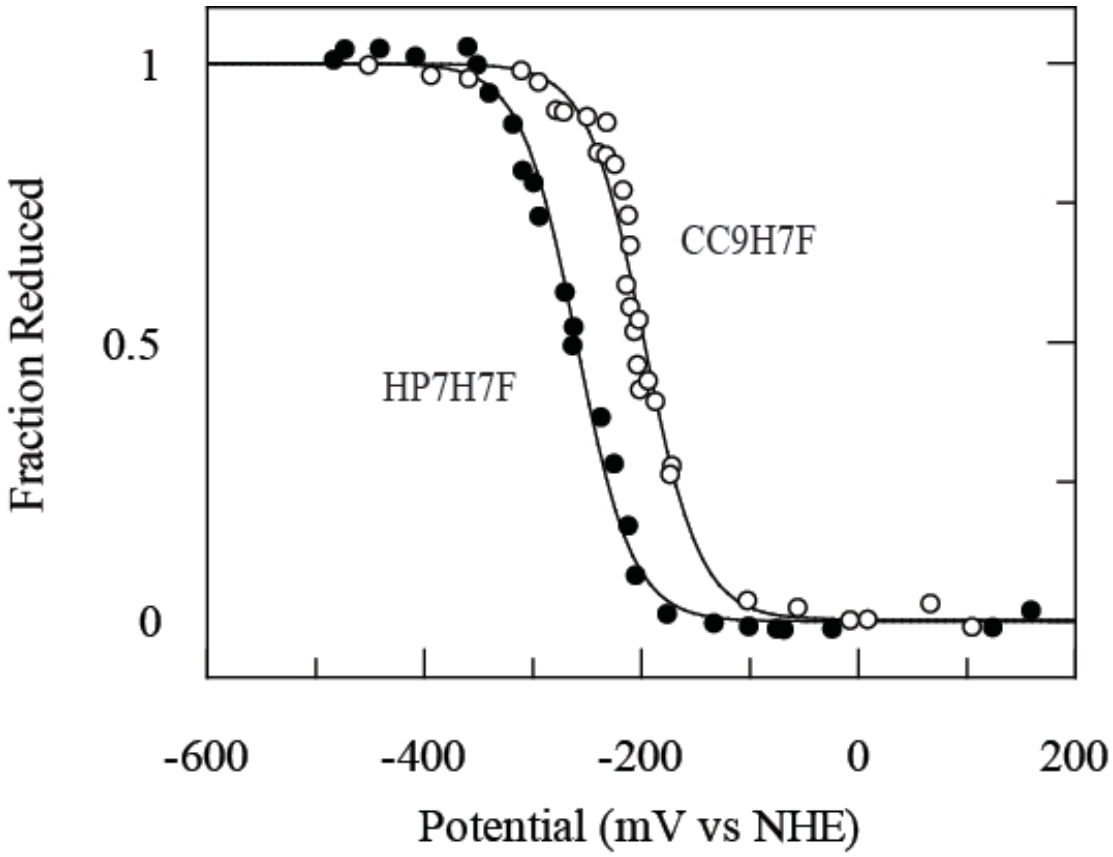

Figure 2.8 Equilibrium potentiometric determination of the electron affinities HP7-H7F and CC9-H7F. Lines drawn are fits with Eqn. 6.

NMR titration of the histidine pK_a. Histidine residues can protonate, and the resultant histidine cation cannot bind heme. This proton competition effect is another possible explanation for the loss of binding affinity in the triple mutant protein (*39*). To determine whether this is the case, NMR was used to determine the pK_a of the molten globular apoprotein histidine ligands. Both protein's histidine pKa's were well below the solution pH (9.0) used in the binding titrations (Figure 9A-D), with that of CC9-H7F approaching the solution pK_a for free histidine, therefore the observed differences in heme K_d are not a consequence of proton competition.

Based on the crystal (*14*) and NMR (*41*) structures of the progenitor protein BB in its apo form, the apoprotein forms of HP7-H7F and CC9-H7F can be expected to take a conformation in which the histidine side chains are buried in the protein core and the b-position residues exposed on the surface. Given this solvent exposure, it is unsurprising that the removal of six negatively charged side chains has such a small effect on the histidine pK_a. In the heme-bound state, however, b-position residues rotate into the low-dielectric hydrophobic core (Figure 1B) and electrostatic coupling has a larger effect, as demonstrated by the change in reduction potentials between the two proteins.

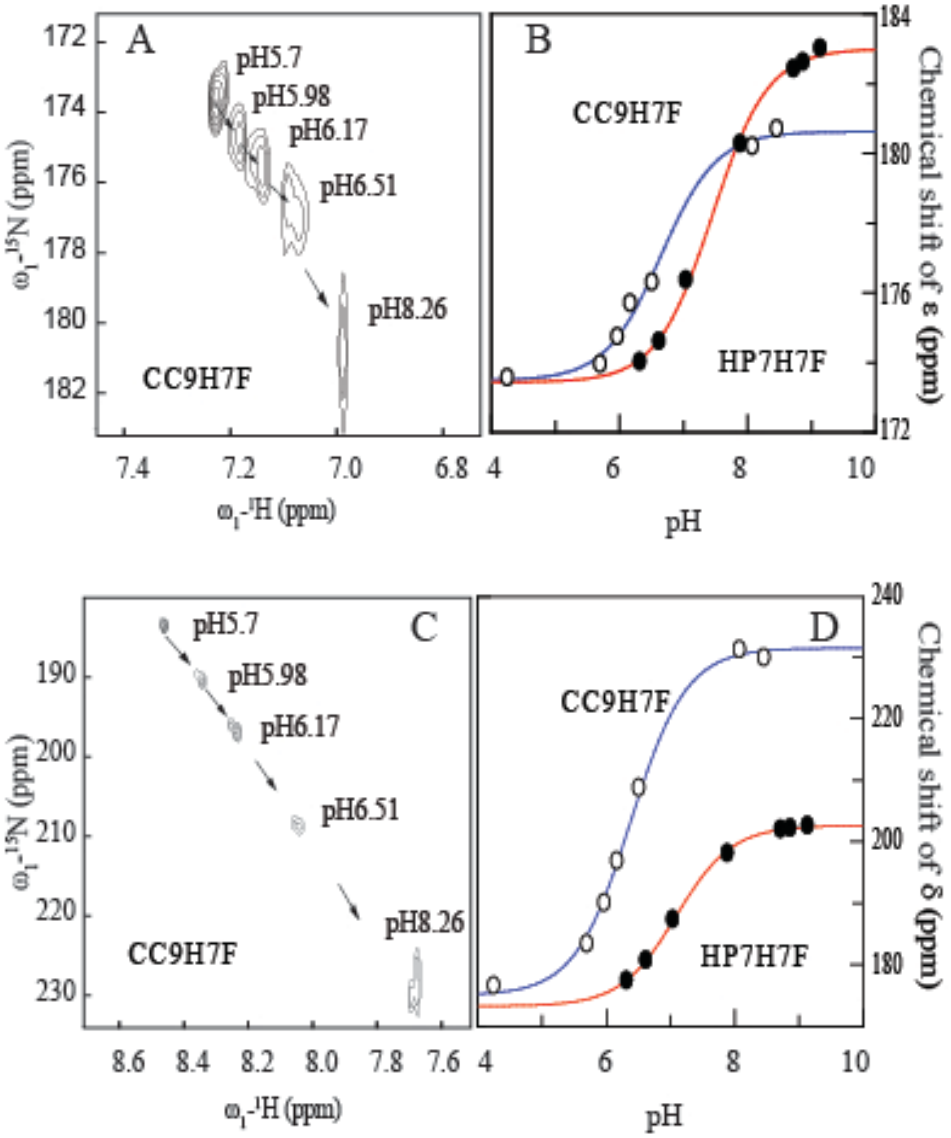

Figure 2.9 NMR determination of the pKas of the histidine ligands in apo-HP7-H7F and apo-CC9-H7F and) NMR determination of the pKas of the histidine ligands in apo-HP7-H7F and apo-CC9-H7F.. (A) Overlay of multiple-bond correlated 1H-15N spectra as a function of pH, showing the titration of the imidazole Hε1-Nε2, signals of histidine side chains. (B) Fits of the 15Nε2 chemical shifts with eqn. 7. (C) Overlay of multiple-bond correlated ^{1}H-^{15}N spectra as a function of pH, showing the titration of the imidazole H$^{\varepsilon 1}$-N$^{\delta 1}$, signals of histidine side chains. (D) Fits of the ^{15}N$^{\delta 1}$ chemical shifts with eqn. 7.

The origin of the difference in heme affinities in the two proteins. Heme binding in hexacoordinate hemoglobins is a three state process consisting of the apoprotein, a pentacoordinate bound state and a hexacoordinate bound state (Figure 10A-C), with the latter two states considered bound states. Binding affinity in such a case was first examined by Morrison and coworkers in their analysis of slow, tight binding enzyme inhibition (*42*). Extending this model to the hexacoordinate hemoglobins gives the relation:

(8) $$K_d = \frac{k_2}{k_1}\left(\frac{k_{-His}}{k_{-His}+k_{+His}}\right)$$

where the ratio k_2/k_1 is $K_{d,pent}$, the dissociation constant which reflects the two-state energy difference between the apo state and the pentacoordinate state, and the term in brackets represents the additional binding energy conferred by distal histidine ligation. Combining the experimental ferrous binding constant with the distal histidine ligation rate constants allows the calculation of $K_{d,pent}$ (Table 2).

These values explain the increase in dissociation constant in CC9-H7F – $K_{d,pent}$ is increased by more than a factor of 60 by the triple mutation. An energy diagram which relates the relative energies of each of these states is depicted in Figure 10D. This graphically demonstrates that the increased affinity of the distal histidine incompletely compensates for the large loss in interaction energy of the pentacoordinate state. The structural origin of this loss in affinity is unclear. One

possibility is that in the pentacoordinate state the b-position glutamate side chains on the helix with the distal (detached) histidine form Van der Waals interactions with the bound heme, and the removal of these side chains therefore weakens the shape complementarity of the binding site. Another possibility is similar behavior in helix containing the proximal (attached) histidine ligand. These differing possibilities point to the limitations inherent in the homodimeric candelabra scaffold. It may be that a single chain protein (*43*), which allows the independent optimization of each helix independent of the other will allow both heme binding and distal histidine coordination to be optimized independently.

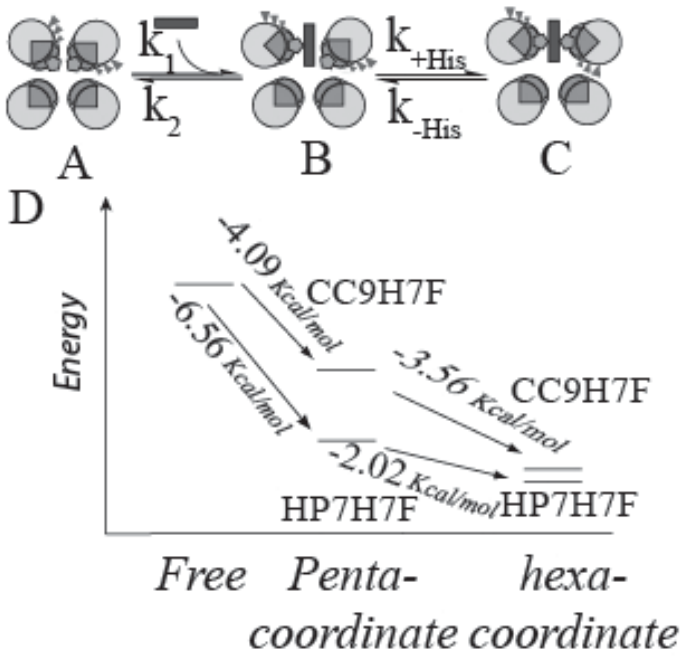

Figure 2.10 Comparative energy levels of the binding states of the two proteins. (A-C) Detail of the binding mechanism: heme binding initially occurs via a pentacoordinate encounter complex (B) which is followed by a protein conformational change driven by distal histidine attachment, resulting in the hexacoordinate, bis-histidine bound state (C). (D) Energy level diagram depicting the relative energies of each of these states in the two proteins.

Section 2.5: Conclusion

The detailed analysis presented here, of the effects of the mutational manipulation of the entatic state energy in our artificial neuroglobin, point to the difficulties inherent in the design and optimization of a functional protein with several conformational and oxidation states. Recent progress in the protein design field has made the creation of a natively structured, high affinity ferric heme protein relatively straightforward, but functional proteins will necessarily require high cofactor affinity in, at the least, both the ferric and ferrous oxidation states of the heme cofactor. Early successes in the design of ferric heme binding proteins took advantage of the strong ferric iron-histidine interaction, estimated to be as high as six kcal/mol (*44*). These interactions are much weaker, however, in the ferrous state (*40*), and high affinity binding of reduced heme and porphyrin cofactors in designed proteins will require a much more sophisticated combination of stabilizing interactions such as binding site complementarity, electrostatic pairing, and heme ligand rotamer optimization (*16,45*).

Section 2.6: Footnotes

[1]Abbreviations used: CO, carbon monoxide; HSQC , heteronuclear single quantum coherence; NHE, normal hydrogen electrode; O_2, molecular oxygen

Section 2.7: Acknowledgement

The authors thank Brian Gibney of the Department of Chemistry, Brooklyn College for many helpful discussions and Hsin Wang, of the Department of Chemistry, the City College of New York, for assistance with NMR measurements. RLK gratefully acknowledges support by the following grants: MCB-0920448 from the National Science Foundation, infrastructure support from P41 GM-66354 to the New York Structural Biology Center and the NIH National Center for Research Resources to CCNY (NIH 5G12 RR03060). PLD gratefully acknowledges support from NIH grant GM-41048. IA and CN gratefully acknowledge support from the NIH's Minority Access to Research Careers program (T34GM007639). ACM gratefully acknowledges support from the Center for Exploitation of Nanostructures in Sensor and Energy Systems (CENSES) under NSF Cooperative Agreement Award Number 0833180.JLRA was supported by a Royal Society Fellowship.

Section 2.8: Reference

1. Sheng, H., Yang, W., Fukuda, S., Tse, H. M., Paschen, W., Johnson, K., Batinic-Haberle, I., Crapo, J. D., Pearlstein, R. D., Piganelli, J., and Warner, D. S. (2009) Long-term neuroprotection from a potent redox-modulating metalloporphyrin in the rat, Free Radic. Biol. Med. 47, 917-923.

2. Koder, R. L., and Dutton, P. L. (2006) Intelligent design: the de novo engineering of proteins with specified functions, Dalton Transactions 25, 3045-3051.

3. Lu, Y. (2005) Design and engineering of metalloproteins containing unnatural amino acids or non-native metal-containing cofactors, Current Opinion in Chemical Biology 9, 118-126.

4. Robertson, D. E., Farid, R. S., Moser, C. C., Urbauer, J. L., Mulholland, S. E., Pidikiti, R., Lear, J. D., Wand, A. J., Degrado, W. F., and Dutton, P. L. (1994) Design and Synthesis of Multi-Heme Proteins, Nature 368, 425-431.

5. Choma, C. T., Lear, J. D., Nelson, M. J., Dutton, P. L., Robertson, D. E., and Degrado, W. F. (1994) Design of a Heme-Binding 4-Helix Bundle, Journal of the American Chemical Society 116, 856-865.

6. Cowley, A. B., Kennedy, M. L., Silchenko, S., Lukat-Rodgers, G. S., Rodgers, K. R., and Benson, D. R. (2006) Insight into heme protein redox potential control and functional aspects of six-coordinate ligand-sensing

heme proteins from studies of synthetic heme peptides, Inorganic Chemistry 45, 9985-10001.

7. Reedy, C. J., and Gibney, B. R. (2004) Heme protein assemblies, Chemical Reviews 104, 617-649.

8. Cowley, A. B., and Benson, D. R. (2007) Weak-field anions displace the histidine ligand in a synthetic heme peptide but not in N-acetylmicroperoxidase-8: Possible role of heme geometry differences, Inorganic Chemistry 46, 48-59.

9. Trent, J. T., Hvitved, A. N., and Hargrove, M. S. (2001) A model for ligand binding to hexacoordinate hemoglobins, Biochemistry 40, 6155-6163.

10. Koder, R. L., Anderson, J. L. R., Solomon, L. A., Reddy, K. S., Moser, C. C., and Dutton, P. L. (2009) Design and engineering of an O2 transport protein, Nature 458, 305-309.

11. Anderson, J. L. R., Koder, R. L., Moser, C. C., and Dutton, P. L. (2008) Controlling complexity and water penetration in functional de novo protein design, Biochemical Society Transactions 36, 1106-1111.

12. Koder, R. L., Valentine, K. G., Cerda, J. F., Noy, D., Smith, K. M., Wand, A. J., and Dutton, P. L. (2006) Native-like structure in designed four helix

bundles driven by buried polar interactions, Journal of the American Chemical Society 128, 14450-14451.

13. Huang, S. S., Koder, R. L., Lewis, M., Wand, A. J., and Dutton, P. L. (2004) The HP-1 maquette: From an apoprotein structure to a structured hemoprotein designed to promote redox-coupled proton exchange, Proceedings of the National Academy of Sciences of the United States of America 101, 5536-5541.

14. Huang, S. S., Gibney, B. R., Stayrook, S. E., Dutton, P. L., and Lewis, M. (2003) X-ray Structure of a Maquette Scaffold, J. Mol. Biol. 326, 1219-1225.

15. Discher, B. M., Koder, R. L., Moser, C. C., and Dutton, P. L. (2003) Hydrophilic to Amphiphilic Design in Redox Protein Maquettes, *Current Opinion in Chemical Biology 7*, 741-748.

16. Negron, C., Fufezan, C., and Koder, R. L. (2009) Helical Templates for Porphyrin Binding in Designed Proteins, *Proteins-Structure Function And Bioinformatics 74*, 400-416.

17. Hecht, M. H., Das, A., Go, A., Bradley, L. H., and Wei, Y. N. (2004) De novo proteins from designed combinatorial libraries, Protein Science 13, 1711-1723.

18. Kamtekar, S., Schiffer, J. M., Xiong, H. Y., Babik, J. M., and Hecht, M. H. (1993) Protein Design by Binary Patterning of Polar and Nonpolar Amino-Acids, Science 262, 1680-1685.

19. Moffet, D. A., and Hecht, M. H. (2001) De novo proteins from combinatorial libraries, *Chemical Reviews 101*, 3191-3203.

20. Wei, Y. N., Kim, S., Fela, D., Baum, J., and Hecht, M. H. (2003) Solution structure of a de novo protein from a designed combinatorial library, Proceedings of the National Academy of Sciences of the United States of America 100, 13270-13273.

21. Wei, Y. N., Liu, T., Sazinsky, S. L., Moffet, D. A., Pelczer, I., and Hecht, M. H. (2003) Stably folded de novo proteins from a designed combinatorial library, Protein Science 12, 92-102.

22. Vallee, B. L., and Williams, R. J. P. (1968) Metalloenzymes - entatic nature of their active sites, *Proceedings Of The National Academy Of Sciences Of The United States Of America 59*, 498-+.

23. Brunori, M., Giuffre, A., and Sarti, P. (2005) Cytochrome c oxidase, ligands and electrons, *Journal Of Inorganic Biochemistry 99*, 324-336.

24. Pace, C. N., Vajdos, F., Fee, L., Grimsley, G., and Gray, T. (1995) How to Measure and Predict the Molar Absorption-Coefficient of a Protein, Protein Science 4, 2411-2423.

25. Dutton, P. L. (1978) Redox potentiometry: determination of midpoint potentials of oxidation- reduction components of biological electron-transfer systems, Methods in Enzymology 54, 411-435.

26. Andrade, M. A., Chacon, P., Merelo, J. J., and Moran, F. (1993) Evaluation of secondary structure of proteins from UV circular-dichroism spectra using an unsupervised learning neural network, Protein Eng. 6, 383-390.

27. Hargrove, M. S. (2000) A flash photolysis method to characterize hexacoordinate hemoglobin kinetics, Biophysical Journal 79, 2733-2738.

28. Berry, E. A., and Trumpower, B. L. (1987) Simultaneous determination of hemes-A, hemes-B, and hemes-C from pyridine hemochrome spectra, Analytical Biochemistry 161, 1-15.

29. Delaglio, F., Grzesiek, S., Vuister, G., Zhu, G., Pfeifer, J., and Bax, A. (1995) NMRPipe: A Multidimensional Spectral Processing System Based on UNIX Pipes, J. Biomol. NMR 6, 277-293.

30. Goddard, T. D., and Kneller, D. G. (2007) Sparky, The University of California, San Francisco.

31. Kay, L. E., Keifer, P., and Saarinen, T. (1992) Pure Absorption Gradient Enhanced Heteronuclear Single Quantum Correlation Spectroscopy with Improved Sensitivity, J. Am. Chem. Soc. 114, 10663-10665.

32. Pelton, J. G., Torchia, D. A., Meadow, N. D., and Roseman, S. (1993) Tautomeric states of the active-site histidines of phosphorylated and unphosphorylated III(GLC), a signal-transducing protein from escherichia coli, using 2-dimensional heteronuclear NMR techniques, Protein Science 2, 543-558.

33. Nanda, V., and Koder, R. L. (2010) Designing artificial enzymes by intuition and computation, Nature Chemistry 2, 15-24.

34. Lyu, P. C., Liff, M. I., Marky, L. A., and Kallenbach, N. R. (1990) Side-Chain Contributions To The Stability Of Alpha-Helical Structure In Peptides, Science 250, 669-673.

35. Ogihara, N. L., Ghirlanda, G., Bryson, J. W., Gingery, M., DeGrado, W. F., and Eisenberg, D. (2001) Design of three-dimensional domain-swapped dimers and fibrous oligomers, Proceedings Of The National Academy Of Sciences Of The United States Of America 98, 1404-1409.

36. Dunbrack, R. L., and Karplus, M. (1993) Backbone-Dependent Rotamer Library for Proteins - Application to Side-Chain Prediction, Journal of Molecular Biology 230, 543-574.

37. Ascenzi, P., Bocedi, A., de Sanctis, D., Pesce, A., Bolognesi, M., Marden, M. C., Dewilde, S., Moens, L., Hankeln, T., and Burmester, T. (2004) Neuroglobin and cytoglobin - Two new entries in the hemoglobin superfamily, Biochem. Mol. Biol. Educ. 32, 305-313.

38. Du, W. H., Syvitski, R., Dewilde, S., Moens, L., and La Mar, G. N. (2003) Solution H-1 NMR characterization of equilibrium heme orientational disorder with functional consequences in mouse neuroglobin, Journal of the American Chemical Society 125, 8080-8081.

39. Reddi, A. R., Reedy, C. J., Mui, S., and Gibney, B. R. (2007) Thermodynamic investigation into the mechanisms of proton-coupled electron transfer events in heme protein maquettes, Biochemistry 46, 291-305.

40. Reedy, C. J., Kennedy, M. L., and Gibney, B. R. (2003) Thermodynamic characterization of ferric and ferrous haem binding to a designed four-alpha-helix protein, Chemical Communications, 570-571.

41. Skalicky, J. J., Gibney, B. R., Rabanal, F., Urbauer, R. J. B., Dutton, P. L., and Wand, A. J. (1999) Solution structure of a designed four-alpha-helix bundle maquette scaffold, Journal of the American Chemical Society 121, 4941-4951.

42. Sculley, M. J., and Morrison, J. F. (1986) The determination of kinetic constants governing the slow,tight-binding inhibition of enzyme-catalyzed reactions, Biochimica et Biophysica Acta 874, 44-53.

43. Bender, G. M., Lehmann, A., Zou, H., Cheng, H., Fry, H. C., Engel, D., Therien, M. J., Blasie, J. K., Roder, H., Saven, J. G., and DeGrado, W. F. (2007) De novo design of a single-chain diphenylporphyrin metalloprotein, Journal Of The American Chemical Society 129, 10732-10740.

44. Shifman, J. M., Moser, C. C., Kalsbeck, W. A., Bocian, D. F., and Dutton, P. L. (1998) Functionalized de novo designed proteins: Mechanism of proton coupling to oxidation/reduction in heme protein maquettes, *Biochemistry 37*, 16815-16827.

45. Braun, P., Goldberg, E., Negron, C., von Jan, M., Xu, F., Nanda, V., Koder, R. L., and Noy, D. (2011) Design principles for chlorophyll-binding sites in helical proteins, *Proteins-Structure Function And Bioinformatics 79*, 463-476.

Chapter 3: Factors Affecting Gaseous Ligand Binding in an Artificial Neuroglobin

Section 3.1: Summary

We report the functional analysis of an artificial hexacoordinate oxygen transport protein, HP7, which operates via a mechanism similar to that of human neuroglobin and cytoglobin: the destabilization of one of two heme-ligating histidine residues. In the case of HP7 this is the result of the coupling of histidine side chain ligation with the burial of three charged glutamate residues on the same helix. We have previously shown that replacement of these glutamate residues with alanine increases the affinity of the distal histidine ligand by a factor of thirteen while decreasing the overall cofactor binding affinity (Zhang et al, Biochemistry **50**(47): 10254-10261). Here we examine the effects these mutations have on function. The K_d of the nonnreactive oxygen analogue carbon monoxide (CO) is only decreased three-fold, despite the large increase in distal histidine affinity engendered by the 22-fold decrease in the histidine ligand off-rate. This is a result of the four-fold increase in affinity for CO binding to the pentacoordinate state. Oxygen binds to HP7 with a K_d of 117 μM, while the mutant rapidly oxidizes when exposed to oxygen. EPR analysis of both ferric hemoproteins demonstrates that the mutation increases disorder at the heme binding site. NMR-detected deuterium exchange demonstrates that the mutation causes a large increase in water penetration into the protein core. The inability of the mutant protein may thus either be due to increased water penetration, the large decrease in binding rate caused by the increase in distal histidine

affinity, or a combination of the two factors.

Section 3.2: Introduction

The first step in oxygen activation and/or transport by heme proteins is the binding of molecular oxygen to the ferrous heme iron while avoiding heme oxidation. It is therefore critical to understand the underlying engineering parameters necessary for this process in order to design artificial oxygen utilizing heme proteins. Furthermore, many enzymes which utilize molecular oxygen as a substrate contain a number of redox-active cofactors in addition to the active site heme. Many of these, for example the heme cofactors in the cytochrome c oxidase, serve to transport electrons into the O_2-utilizing heme A-containing active site (*1*). Thus it will further be necessary in the future design of more complex artificial catalysts to be able to restrict ligand binding to those sites where catalysis is intended.

The family of hexacoordinate hemoglobins are oxygen activating enzymes characterized by the property that they are bis-histidine-ligated in the oxidized state and exist in a mixed bis- and mono-histidine ligation state when reduced (*2*). The transient pentacoordination of the heme cofactor allows for the binding of molecular oxygen. We have recently reported the design, bacterial expression, and biochemical analysis of the completely artificial hexacoordinate oxygen transport protein HP7 (*3*). This protein consists of two heme cofactors bound to a homodimeric four alpha helix bundle protein. Each monomer is in a helix-loop-helix configuration and the two monomers bind to each other via hydrophobic sequestration with the monomer loops on the same end of the protein and attached to each other via a disulfide bond, a topology we have termed the

'candelabra motif' (*4*).

The heme cofactors bind to parallel helices via histidine ligands at the seventh position of each helix, one at the site furthest from the loops (the 'candle' end) and one at the site closest to the loops (the 'loop' end).[2] One of each pair of identical helices which bind a heme cofactor is oriented such that three polar glutamic acid residues must rotate into the hydrophobic core of the protein when the histidine is ligated to the heme iron. This strained, 'entatic' conformation (*5*) relaxes via the detachment of the distal histidine followed by rotation of the helix to move the glutamate side chains into solution, opening a ligation site on the heme iron to bind a gaseous ligand.

HP7 binds two hemes sequentially, the first at the candle end of the protein and the second nearer the loops (*4*). Our initial experiments were performed with HP7 bound to a single heme at the candle end binding site. We then simplified the protein by removing the candle end heme binding site, creating the homodimeric protein HP7-H7F which contains a single hexacoordinate binding site in the loop end of the bundle (*6*). Then, to examine the effects of changes in distal histidine ligand association energy on the overall heme binding affinity, we mutated the three buried glutamate residues on the ligating helix to alanine. This was found to slow the histidine ligand off-rate 22-fold, increase the affinity of the distal histidine ligand by a factor of thirteen and increase the bound cofactor reduction potential by 65 mV. However, it also decreased the heme binding affinity by a factor of five in the reduced

state and 60 in the oxidized state. This was suggested to be caused by the homodimeric nature of the candelabra fold – mutations to the set of glutamates on the distal histidine helix responsible for the entatic state are also necessarily present in the proximal, nonrotating helix. The loss of these side chains greatly weakens binding, as evinced by a 60-fold decrease in the calculated ferrous heme binding constant to the histidine-detached pentacoordinate state, in which distal histidine ligation does not play a factor.

Here we show that by substituting the three strain-inducing glutamate residues we can effectively manipulate the thermodynamics of the entatic state and modulate the affinity and kinetics of CO binding. All designed heme proteins created to date bind CO, and by extrapolation O_2, with varying levels of affinity (*3, 7*). Furthermore, CO is capable of binding to bis-histidine ligated hemes in natural cytochromes B that do not functionally participate in gaseous ligand binding (*8, 9*). We further show that O_2 binds to the starting protein but not the mutant, although we cannot determine whether the inability of the mutant protein to bind O_2 is a result of the greatly slowed rate of histidine ligand detachment or increased water penetration due to the larger degree of disorder caused by the mutation.

Section 3.3: Materials and Methods

Chemicals. Hemin was purchased from Fluka (Buchs, Switzerland). Molecular oxygen (O_2) (99.98% purity), carbon monoxide (CO)[1] (99.9%), and molecular nitrogen (N_2) (99.99%) gases were from Matheson Gas (Basking Ridge, NJ) and the latter two were scrubbed of residual O_2 by passage through two bubblers filled with a reduced vanadium sulfate solution followed by another filled with water (*10*). PD-10 desalting columns were from GE Healthcare (Port Washington, NY). All other solvents and reagents were from either Fisher Scientific or Sigma.

General biochemistry. The proteins HP7-H7F and CC9-H7F were expressed and purified and heme complexes were formed as described earlier (*6*). Optical spectra were collected with a Hewlett-Packard (New York, NY) 8452A Diode array spectrophotometer running the Olis (Bogart, GA) SpectralWorks software and equipped with a Quantum Northwest (Liberty Lake, WA) Peltier temperature controller. All experiments were performed at 20° C in 250mM Boric Acid, 100mM KCl pH 9.0 unless otherwise noted. Each kinetic experiment was performed at least three times and reported errors are standard deviations from the mean.

Kinetic analysis of CO dissociation. The dark dissociation rate of the CO complex was determined using the ferricyanide trapping method of Moffet *et al* (*7*): briefly, anaerobic solutions of carbonmonoxyferrous protein complex were mixed with varying concentrations of potassium ferricyanide. The rates of the linked reactions of CO dissociation followed by heme oxidation by ferricyanide were

followed by monitoring the disappearance of carbonmonoxyferrous Soret peak at 421 nm. Double reciprocal plots of the rates of oxidation *vs.* the concentration of ferricyanide extrapolated to infinite ferricyanide give the inverse CO dissociation rate as given by Eqn. 1:

(1) $$\frac{1}{k} = \frac{k_{on}[CO]}{(k_{ox})(k_{off})}\left(\frac{1}{[FC]}\right) + \frac{1}{k_{off}}$$

Flash photolysis analysis of CO association. The rate constants for both CO and histidine binding to the pentacoordinate state were determined using laser flash photolysis experiments performed as we've described previously (*6*): briefly a 1-ns pulse-width frequency doubled YAG laser at 532 nm excites the preformed carbonmonoxyferrous complex, causing the detachment of the ligand CO. This transiently forms an unliganded pentacoordinate heme protein and the rates of CO rebinding to the pentacoordinate state can be determined by analyzing the multi-exponential rebinding traces taken as a function of CO concentration using the method of Hargrove (*11*):

(2) $$\gamma_1 + \gamma_2 = k_{-H} + k_{+H} + k_{+CO}[CO]$$

Where γ_1 and γ_2 are the fitted first and second CO-dependent exponential rates and the kinetic constants are defined as in Equation 1 with the exception that CO denotes CO-binding rate constants instead of O_2 binding rate constants. Protein concentrations were 20-25 μM and carbonmonoxyferrous complexes were prepared by titrating solutions of the holoproteins with an excess of dithionite as observed by visible spectroscopy under an atmosphere containing 10-100% CO mixed with argon. K_{+CO}

is taken directly from the slope of the replot of the sum of γ_1 and γ_2.

Stopped Flow analysis of O_2 binding and dissociation. Binding kinetics of O_2 with ferrous protein-heme complexes were followed spectroscopically in rapid stopped-flow mixing experiments over gas concentrations from 2% to 50% saturation at 15° C using a Biologic (Lyon, France) SFM 300 stopped flow mixer equipped with either a Biologic MOS 200 absorbance detector for single wavelength detection of a custom-built Olis RSM 1000 spectrometer for multiwavelength detection. Protein concentrations were 20-25 μM and ferrous complexes were prepared by carefully titrating anaerobic solutions of the holoproteins with a slight excess of sodium dithionite as observed by visible spectroscopy. Ferrous samples were anaerobically transferred to the stopped-flow loading syringe by canula. Binding kinetic data were fit with Eqn. 1, which assumes that O_2 binding rate, k_{+O2} , is much greater than the sum of the distal histidine association and dissociation rates (*2*):

$$(3)\quad k_{obs} = \frac{k_{-H} k_{+O2}[O_2]}{k_{+H} + k_{-H} + k_{+O2}[O_2]}$$

Where k_{obs} is the fitted single exponential binding rate, k_{+H} and k_{-H} are the distal histidine-ferrous heme iron association and dissociation rates and k_{+O2} is the O_2 association rate constant. At high $[O_2]$. $k_{obs} = k_{-H}$.

Kinetic analysis of O_2 dissociation. The dark dissociation rate of the O_2 complex was determined in rapid stopped-flow double mixing experiments using the

CO displacement method (*12*). Briefly, the O_2 complex was formed as above by mixing reduced protein and O_2-saturated buffer. After a delay of 100 ms for complex formation this mixture was mixed with a two-fold larger volume of CO-containing buffer. The rate of O_2 displacement by CO was collected over final CO concentrations ranging from 200-600 μM. At high CO concentration, the observed rate of replacement, r_{obs} is given by Eqn. 4:

(4) $r_{obs} = k_{-O_2}/[1 + \left(\frac{k_{+O_2}[O_2]}{k_{+CO}[CO]}\right)]$

Since $k_{+co}[CO] \gg k_{+O2}[O_2]$, the observed replacement rate constant is directly equal to O2 dissociation rate constant, $r_{obs} \approx k_{-O_2}$

Electron paramagnetic resonance (EPR) spectroscopy. Low-temperature (7 K) EPR spectra were recorded on a Bruker E500 ElexSys EPR spectrometer operating at the X-band using an Oxford Spectrostat continuous flow cryostat and ITC503 temperature controller. Data acquisition and manipulation were performed using *XeprView* and *WinEPR* software (Bruker). EPR samples were prepared by pipetting approximately 200 μL of 0.3mM protein solution in 200 mM TRIS-maleate buffer at pH 8.0 into 4 mm (3 mm i.d) precision bore quartz EPR tubes followed by immersion freezing in liquid nitrogen. Experimental parameters used were as follows: modulation amplitude, 4 G; microwave power, 1 mW; modulation frequency, 100 kHz; microwave frequency, 9.39 GHz; scan rate, 14.9 G/s; conversion time, 327 ms;

time constant, 1310 ms; number of scans, 1. All spectra were obtained under identical instrumental conditions.

Nuclear magnetic resonance (NMR) spectroscopy. All NMR experiments were performed at 20^{o}C on Varian Inova spectrometer operating at a 600MHz and equipped with a triple resonance cryogenic probe capable of applying pulse field gradients in the z-direction. Data were processed using the program NMRPipe (*13*) and analyzed using Sparky (*14*). For hydrogen exchange assays, sensitivity enhanced ^{1}H-^{15}N heteronuclear single quantum coherence (HSQC) spectra (*15*) were collected on 50-100 μM ^{15}N-labelled holo- and apoprotein samples with sweep widths of 10,000 Hz for ^{1}H and 2000 Hz for ^{15}N utilizing GARP decoupling of ^{15}N during ^{1}H acquisition. Chemical shifts are referenced to water at 4.77 ppm for ^{1}H.

Hydrogen-Dueterium exchange. ^{15}N-labelled holo- and apoprotein samples of HP7-H7F and CC9-H7F in 25 mM potassium phosphate buffer pH 6.5 were passed through a PD-10 solvent exchange column pre-equilobrated in 25 mM KaD_2PO_4 D_2O buffer pD 6.5 (pH meter reading + 0.4 pH units), immediately placed in a 5mm NMR tube and temperature equilibrated at 20°C for five minutes in the sample compartment of the NMR spectrometer. At this point protein concentrations were approximately 300 μM. The fraction of remaining amide protons remaining was assessed as a function of time by collecting one dimensional HSQC, or isotope selective, ^{1}H spectra.

Oxygen life time determination. Since the affinity of the oxygen is very strong, the free oxygen concentration is significantly depleted when the oxygen bind the protein heme complex, So that we cannot use the approximation that the free oxygen concentration was equal to the total oxygen concentration. The depletion of the oxygen and protein complex concentration must be considered. Through the equation (5) and (6),

$$[P] = [P\cdot O_2]+[P]_{free} \quad (5)$$

$$[O_2]= [P\cdot O_2]+[O_2]_{free} \quad (6)$$

Where the [P] is the total protein heme complex concentration; $[P\cdot O_2]$ is the protein heme-oxy complex concentration; $[P]_{free}$ is the free protein heme complex concentration; $[O_2]$ is the total oxygen concentration; $[O_2]_{free}$ is the free oxygen concentration.

We remake the dissociation constant equation as follows:

$$K_d = \frac{([P]-[P\cdot O_2])([O_2]-[P\cdot O_2])}{[P\cdot O_2]} \quad (7)$$

And convert it as

$$[P\cdot O_2] = \frac{([P]+[O_2]+K_d)-\sqrt{([P]+[O_2]+K_d)^2-4[P][O_2]}}{2} \quad (8)$$

For the second step, the free oxygen oxidized the protein heme complex as below:

$$[P\cdot O_2] \overset{K_d}{\leftrightarrow} [P] + [O_2] \overset{k_{ox}}{\longrightarrow} [P]_{ox}$$

In this case the oxidization rate as known:

$$Rates=K_{ox}[P]_{free} \cdot [O_2]_{free} \quad (9)$$

Combining the equation (7),(8)and (9), the oxidization rate can be expressed as

$$Rates = k_{ox} \cdot K_d \cdot \frac{([P]+[O_2]+K_d)-\sqrt{([P]+[O_2]+K_d)^2-4[P][O_2]}}{2} \quad (10)$$

The existing life time of O_2 bond with ferrous protein-heme complexes were followed spectroscopically in rapid stopped-flow mixing experiments over each gas and air individually concentrations from 16.67% to 66.67% saturation at 16° C using a Biologic (Lyon, France) SFM 300 stopped flow mixer equipped with either a Biologic MOS 200 absorbance detector for single wavelength detection of a custom-built Olis RSM 1000 spectrometer for multiwavelength detection. Protein heme complex concentrations were about 1 μM with 10 folder more apo-protein saturated and ferrous complexes were prepared by carefully titrating anaerobic solutions of the holoproteins with a slight excess of sodium dithionite as observed by visible spectroscopy. Ferrous samples were anaerobically transferred to the stopped-flow loading syringe by canula. Kinetic data were fit with Eqn. 10, which assumes that O_2 bind ferrous protein heme complex and get equilibrium very fast, thus the O_2 dissociated and the free O_2 penetrated into the hydrophobic binding core grab the electron from the ferrous heme, which induced the holoprotein oxidized.

Section 3.4: Results and Discussion

Protein design. HP7 complexed with one heme per homodimer has the candle end binding site occupied (*4*). The HP7-H7F mutation eliminates the candle end binding site but preserves the heme binding site nearest the loops. This enables the analysis and comparison of the the gaseous ligand binding properties of the two proteins in the absence of complicating cooperative effects caused by interactions between the two hemes and the conformational effects, including helical rotation, caused by their binding. The CC9-H7F mutant has the three b-position glutamate residues on the histidine ligand helices of HP7-H7F mutated to alanine.

Rates of CO release. Figure 3.3-3.4 depicts the ferricyanide trapping analysis of CO release in the two proteins. Off-rates differ by a factor of three (see Table 1), which is unsurprising as the CO-bound state already has the distal histidine detached, and is thus unaffected by the stability of the entatic state or the kinetics of histidine release. The slopes of the replots, which are indicative of the rates of electron transfer between the unbound state and ferricyanide (*7*), indicate that this oxidation reaction is slower for CC9-H7F than for HP7-H7F. This could either be a steric effect or a result of the higher reduction potential of the heme bound to CC9-H7F.

CO-flash photolysis determination of $k_{+co,pent.}$ We have previously reported the rebinding kinetics, after laser flash photolysis, of the distal histidine in HP7-H7F and CC9-H7F (*6*). In CC9-H7F, HP7-H7F, and our original analysis of HP7 (*3*), a fast exponential process which is independent of the concentration of CO is observed.

Similar behavior has been observed in mouse neuroglobin, and was ascribed to a relaxation process following a probable rearrangement caused by the change in heme iron planarity induced by detachment of the CO ligand (*16, 17*). In each case two slower exponential processes, each of which varies in rate and magnitude with CO concentration, were also observed. Figure 2A depicts the replots of the sum of these two processes for HP7-H7F and CC9-H7F. Eqn. 2 states that, $k_{+co,pent}$, the binding rate of CO to the pentacoordinate state can be derived from the slopes of these replots.

CO binding rates to the pentacoordinate complex differ only by 30%. This coupled with the CO release rate allows the calculation of the CO affinities for the pentacoordinate states of both proteins: HP7-H7F has a K_d of 300 nM and CC9-H7F has a K_d of 80 nM. The true binding constant for CO to hexacoordinate hemoglobins, which takes into account the hexacoordinate state, is given by the relation (*18*):

(5) $k_{d,CO} = k_{d,CO,pent}(1 + K_{A,his})$

The calculated dissociation constant for CO binding to CC9-H7F is only three fold higher than in HP7-H7F (table 1). The twelve-fold larger histidine affinity is counterbalanced by the higher intrinsic CO affinity of the CC9-H7F heme, resulting in a small overall decrease in CO affinity. CO binds tightly to almost all natural ferrous heme proteins, resulting in a host of physiological effects (*19, 20*). In enzymes, however, slowing the onset of CO binding to rates slower than catalytic turnover is an alternative strategy to avoid CO inhibition – if the heme in question is

only transiently reduced, there is insufficient time for a significant level of CO adduct formation to occur. Thus despite the small decrease in CO affinity the 22-fold slowing of CO binding, to 0.25 s^{-1}, represents a significant improvement.

Table 3.1 Heme iron ligand on- and off-rates and equilibrium constants in 3

Haem Protein	$k_{+co,\ pent}$ ($mM^{-1}s^{-1}$)	k_{-co} (ms^{-1})	$K_{d,\ CO,\ pent}$ (μM)	$K_{d,co}$ (μM)	K_{+his} (s^{-1})	k_{-his} (s^{-1})	$K_{A,his}$
HP7H7F	220±6	66.7±0.2	0.303±0.009	9±2	160±20	5.6±0.3	29±5
CC9H7F	296±9	23±5	0.08±0.02	30±10	94±11	0.25±0.01	380±60
HP7	950	34	0.036	0.68	310	17	18

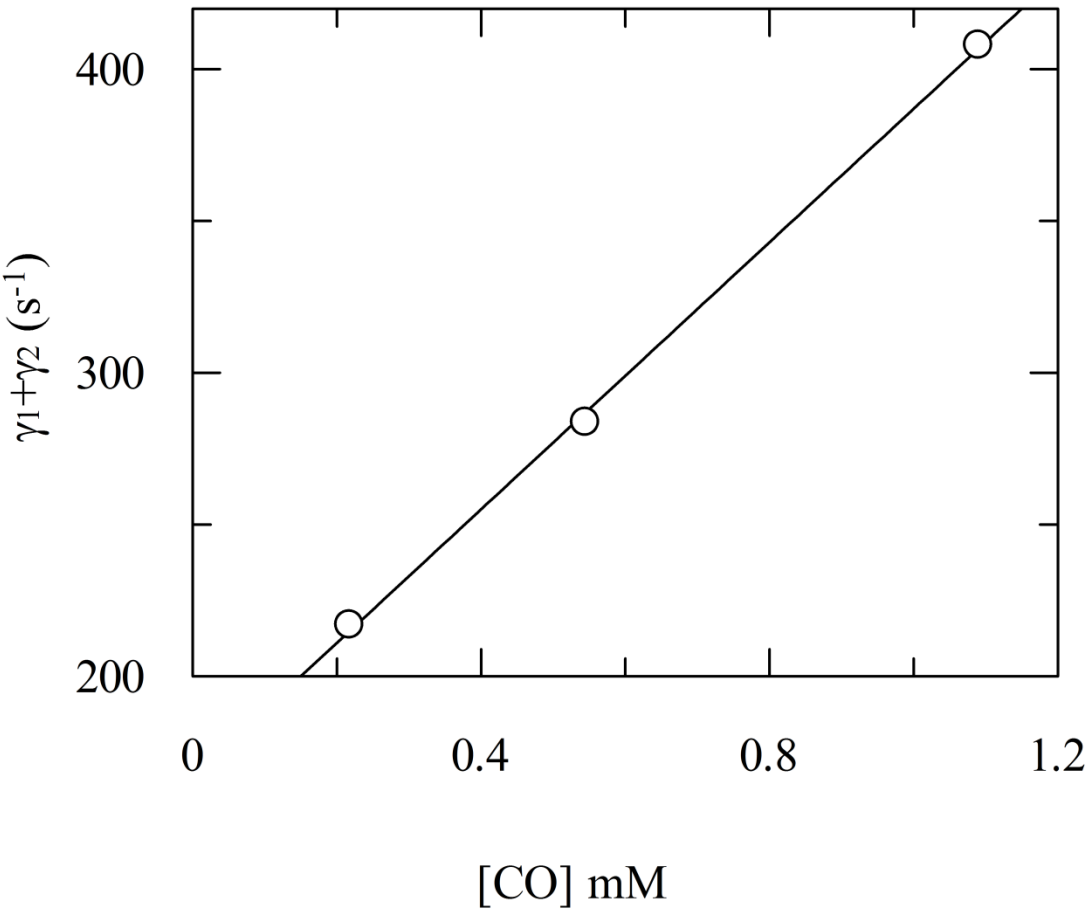

Figure 3.1 Kinetic analysis of CO and histidine binding to HP7-H7F. Laser flash kinetic analysis of histidine and CO rebinding to HP7H7F followed at 419 nm. These data were fit with three exponentials, the first of which represents a [CO]-independent relaxation process. Replots of the sums of the second two exponentials.

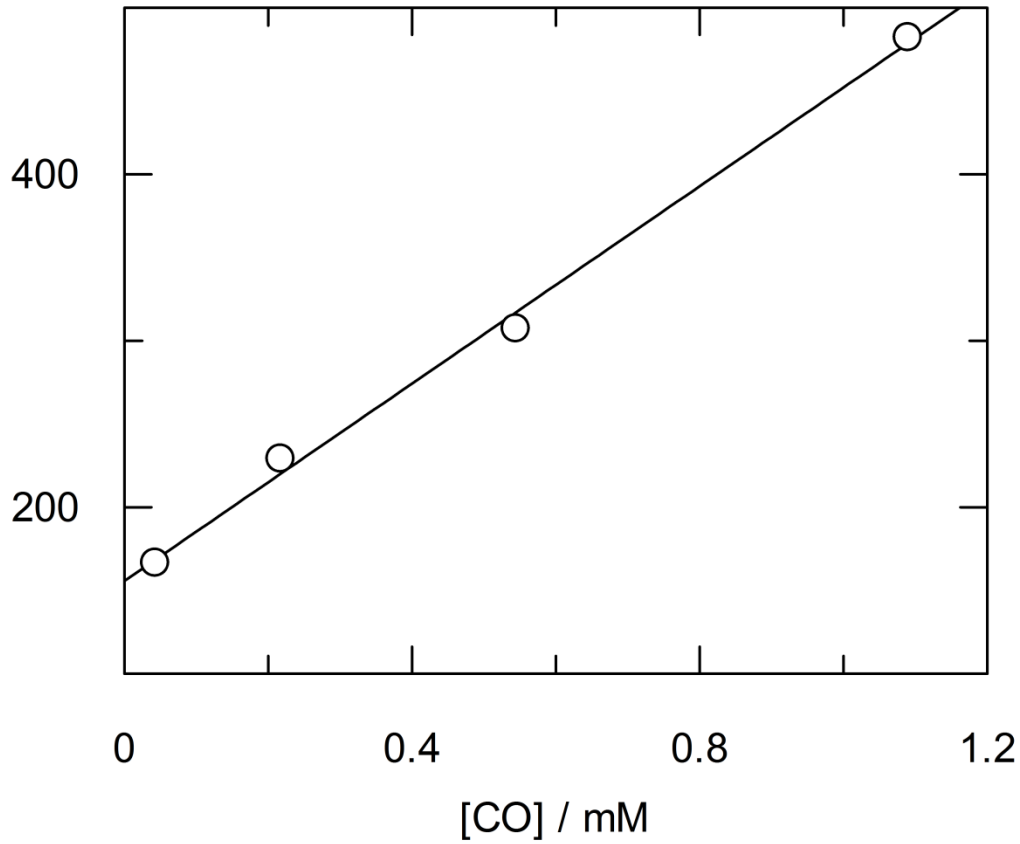

Figure 3.2 Kinetic analysis of CO and histidine binding to CC9-H7F. Laser flash kinetic analysis of histidine and CO rebinding to CC9-H7F followed at 419 nm. These data were fit with three exponentials, the first of which represents a [CO]-independent relaxation process. Replots of the sums of the second two exponentials.

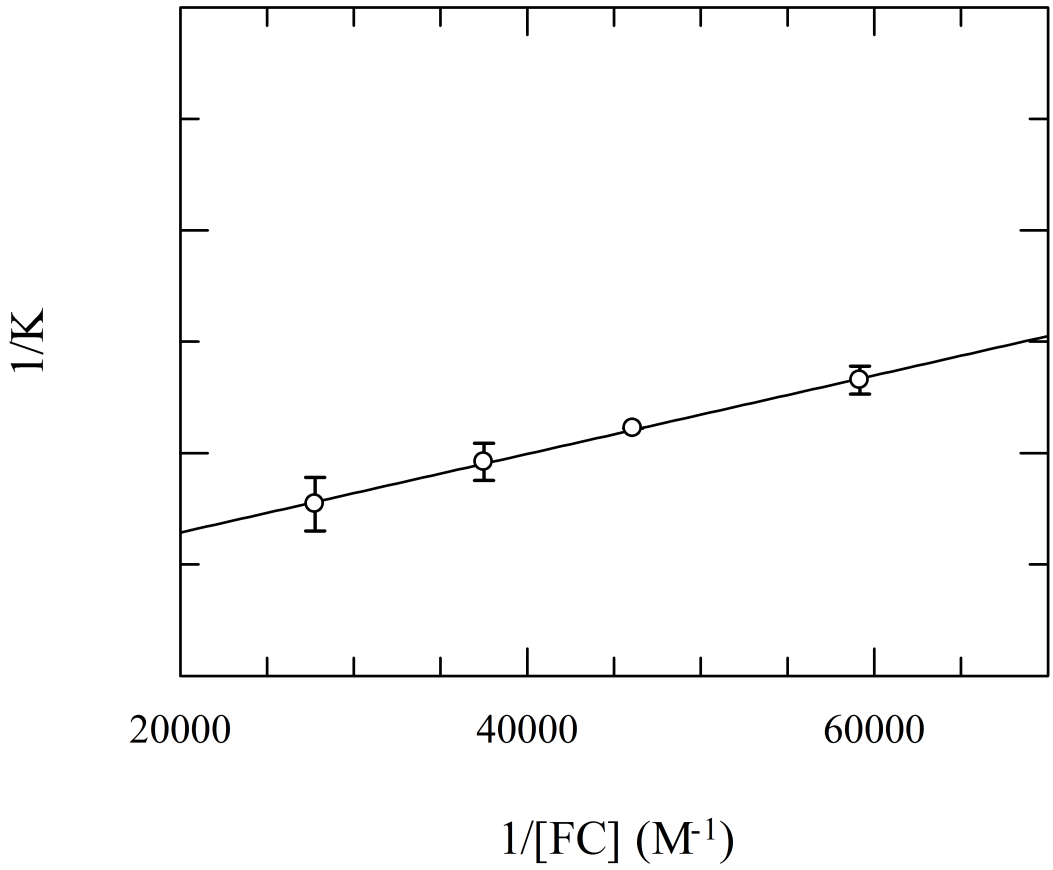

Figure 3.3 Kinetic analysis of CO and histidine binding to HP7-H7F. Ferricyanide trapping analysis of CO release. Double reciprocal plots of the rates of oxidation *vs.* the concentration of ferricyanide extrapolated to infinite ferricyanide give the CO dissociation rate.

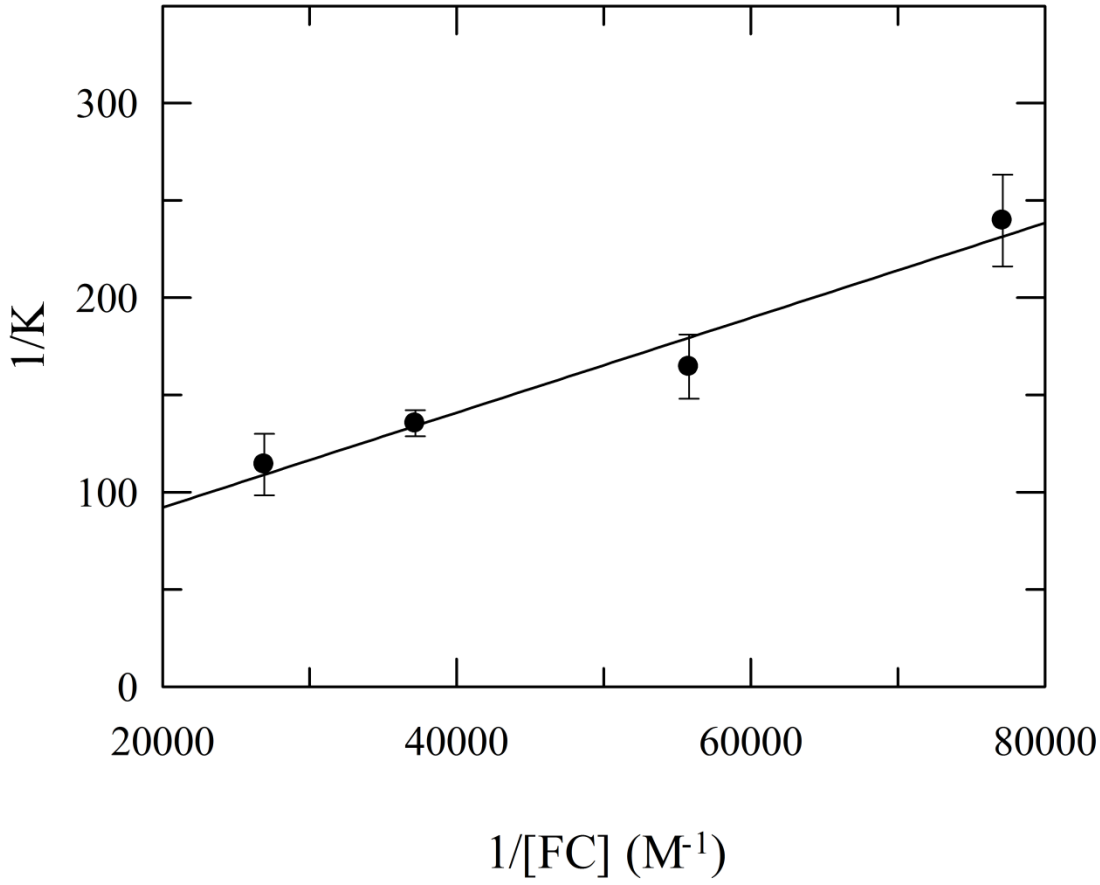

Figure 3.4 Kinetic analysis of CO and histidine binding to CC9H7F. Ferricyanide trapping analysis of CO release. Double reciprocal plots of the rates of oxidation *vs.* the concentration of ferricyanide extrapolated to infinite ferricyanide give the CO dissociation rate.

Rates of O_2 release. Figure3.7-3.8 show the CO replacing analysis of O_2 release in two proteins: HP7H7F and HP7 mono-complex. The UV spectra at -10°C indicate that CC9H7F cannot form the ferrous oxygen complex. Figure 3.5 depicts the Soret peak shift and intensity change between reduced state, oxy-state and oxidized state. The off rates, differing by a factor of three (see table 2), are offset by the on rates, showing negligible difference between the oxygen binding of the two histidine binding sites.

Electron paramagnetic resonance (EPR) spectroscopy. Figure 3.9 depicts a low spin system analysis of the ferric complex in HP7H7F and CC9H7F. Multiple low spin g factors in CC9H7F indicate higher structural flexibility, which is congruous with our expected design. The side chain mutation resulted in higher water penetration due to the increased CC9H7F core hydrophilicity and diminished structural rigidity.

Hydrogen-Deuterium exchange. Figure 3.10 depicts the water penetration in HP7H7F and CC9H7F. The 1D N^{15}-HSQC spectra as a function of time shows the rapid hydrogen-deuterium exchange in both apo-proteins due to their random coil structures. With heme binding, CC9H7F exhibits the same exchange rate as the apo-protein. The longer penetration time of HP7H7F complex in comparison to CC9H7F indicates that side-chain rotation into binding core can increase core hydrophobicity and slow gaseous ligands transfer.

Oxygen life time determination. Figure 3.11-3.12 depicts the oxidization rates of HP7H7F and HP7 mono-histidine oxygen binding. The two different histidine binding sites demonstrate similar observed chemical reaction rates, which depend on both the oxidation and oxygen dissociation rates. The oxygen dissociation rates derived from Figure 3.11-3.12 support the stopped flow analysis described above. The oxidization rate of the HP7H7F ferrous heme complex is half the HP7 mono-complex, attributable to the loop nearby the histidine binding site.

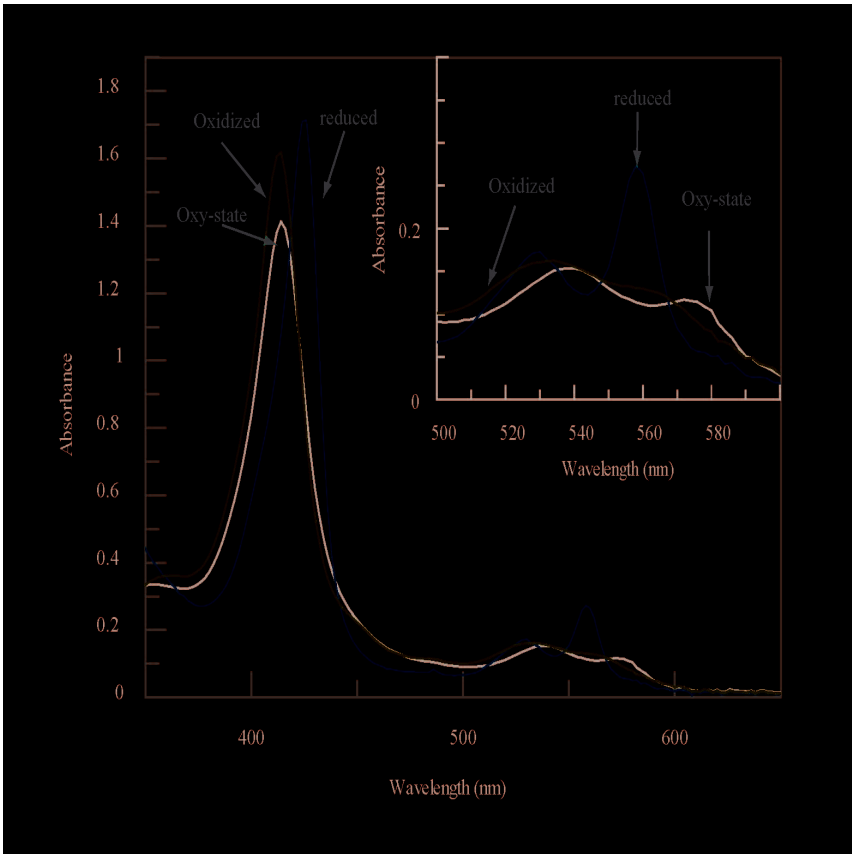

Figure 3.5 UV-VIS spectra of oxidized(blue), reduced(red line) and oxygen bond HP7H7F heme complex. when holoprotein was mixed with small amount oxygen saturate buffer, the sharp Soret peak moved from 428nm to 412nm, and in the Q-band area the remarkable peak at 558nm decreased rapidly meanwhile the peak at 572nm slightly increased initiated by the oxygen binding

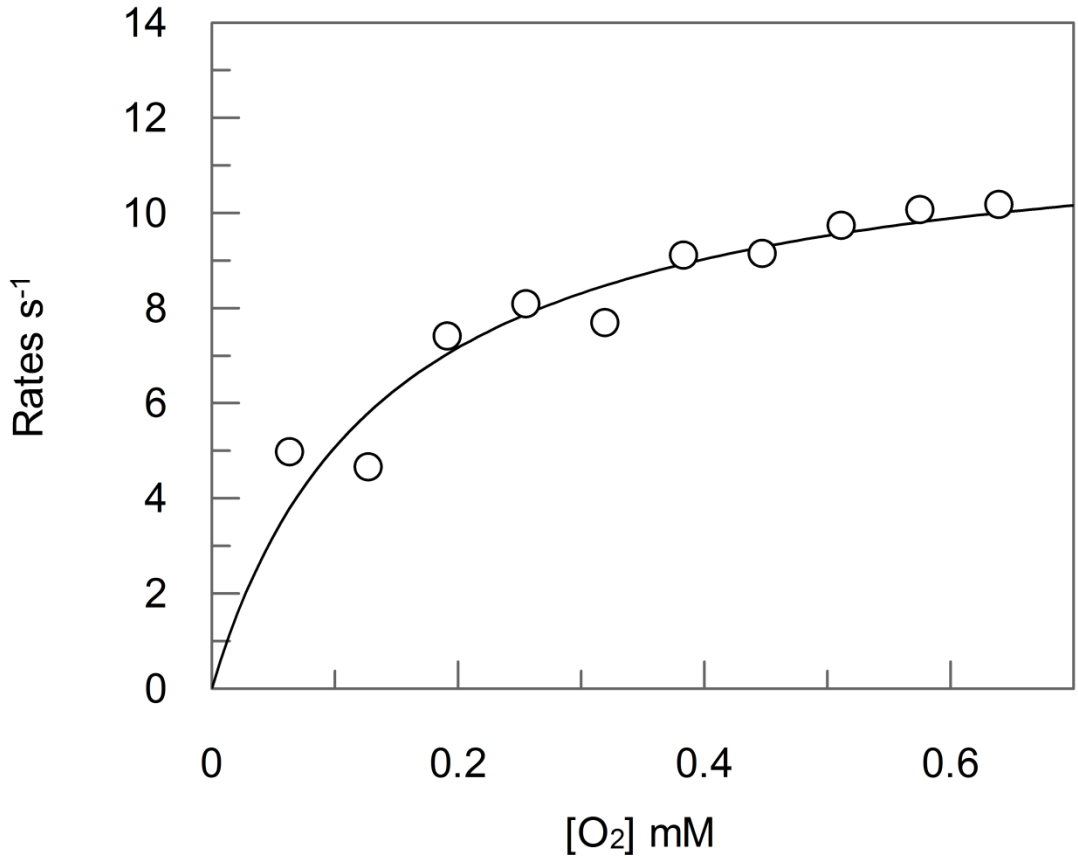

Figure 3.6 Kinetic analysis of O_2 and histidine binding to HP7-H7F. Stopped-flow analysis of the rates of O_2 binding to reduced heme proteins as a function of ligand concentration. Lines are fits with eqn. 3.

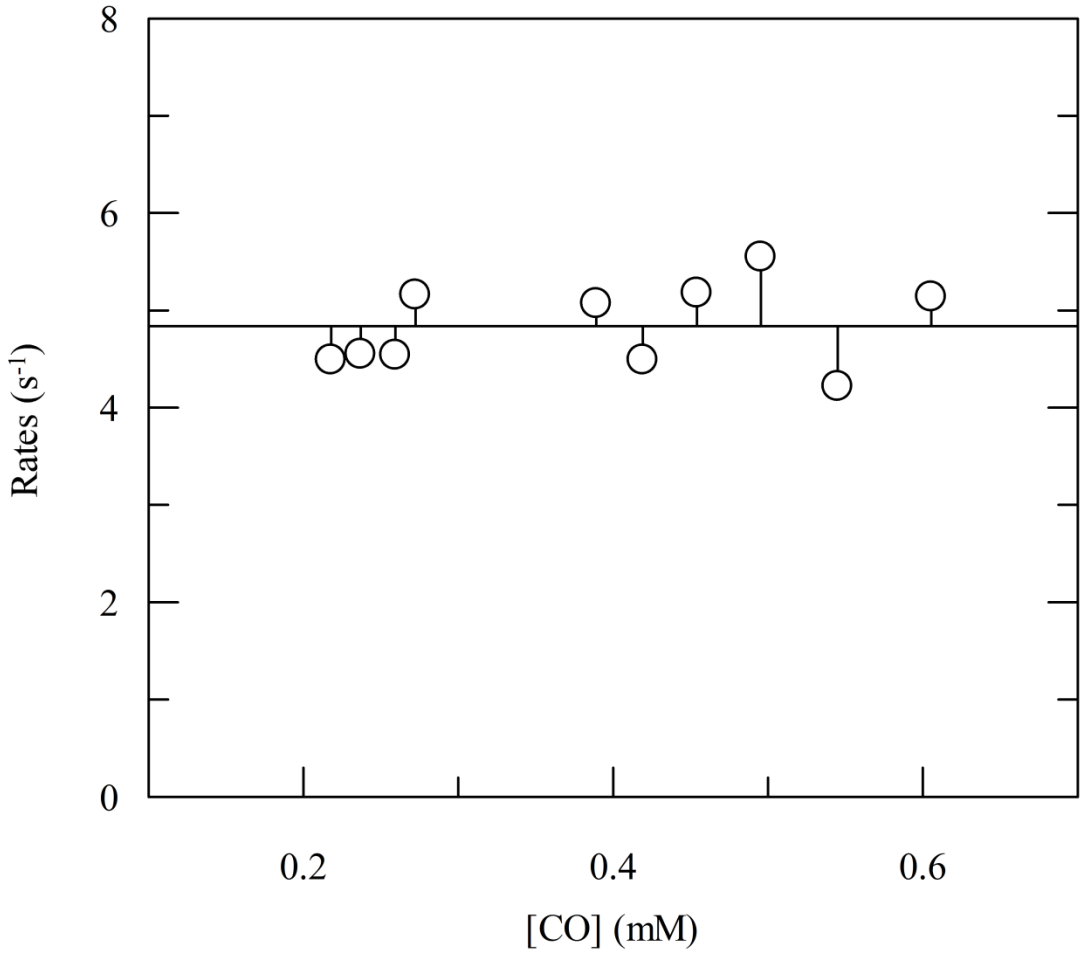

Figure 3.7 Kinetic analysis of O_2 and histidine binding to HP7-H7F. Stopped-flow analysis of the rates of O_2 release replaced by carbon monoxide to increase absorbance at specific wavelength 420nm as a function of time. Double reciprocal plots of the observed rates *vs.* the concentration of carbon monoxide give the O_2 dissociation rate as a constant value.

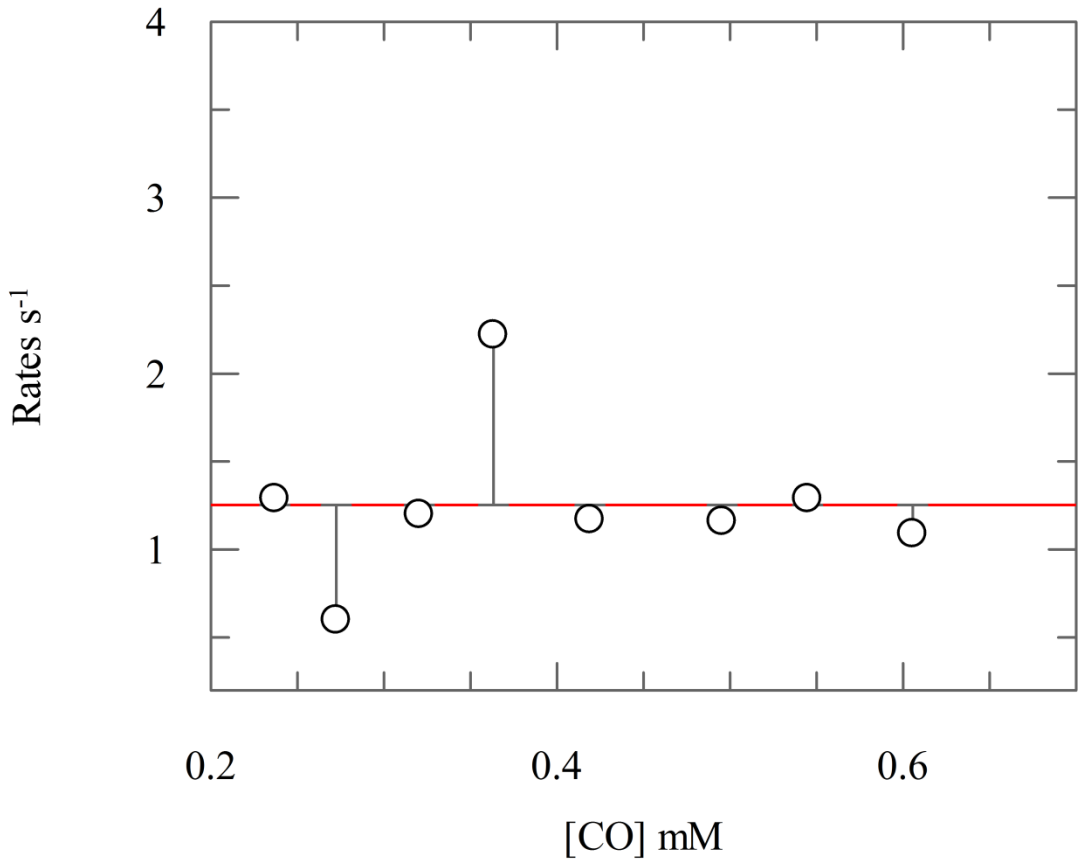

Figure 3.8 Kinetic analysis of O_2 and mono-histidine binding to HP7. Stopped-flow analysis of the rates of O_2 release replaced by carbon monoxide to increase absorbance at specific wavelength 420nm as a function of time. Double reciprocal plots of the observed rates *vs.* the concentration of carbon monoxide give the O_2 dissociation rate as a constant value.

Table 3.2	Haem iron ligand on- and off-rates and equilibrium constants in 3 artificial proteins							
Haem Protein	ligation	$k_{o2\ on}$ ($mM^{-1}s^{-1}$)	$k_{o2\ off}$ (s^{-1})	$K_{d\ O2\_pen}$ (μM)	K_{dO2_actual} (μM)	$k_{his\ on}$ (s^{-1})	$k_{his\ off}$ (s^{-1})	$K_{A,his}$
HP7H7F	Bis-His42	1200±200	4.8±0.4	3.9±0.9	120±50	160±20	5.6±0.3	29±5
CC9H7F	Bis-His42	n/a	n/a	n/a	n/a	94±11	0.25±0.01	380±60
HP7	Bis-His7	310	1.25	4	77	310	17	18

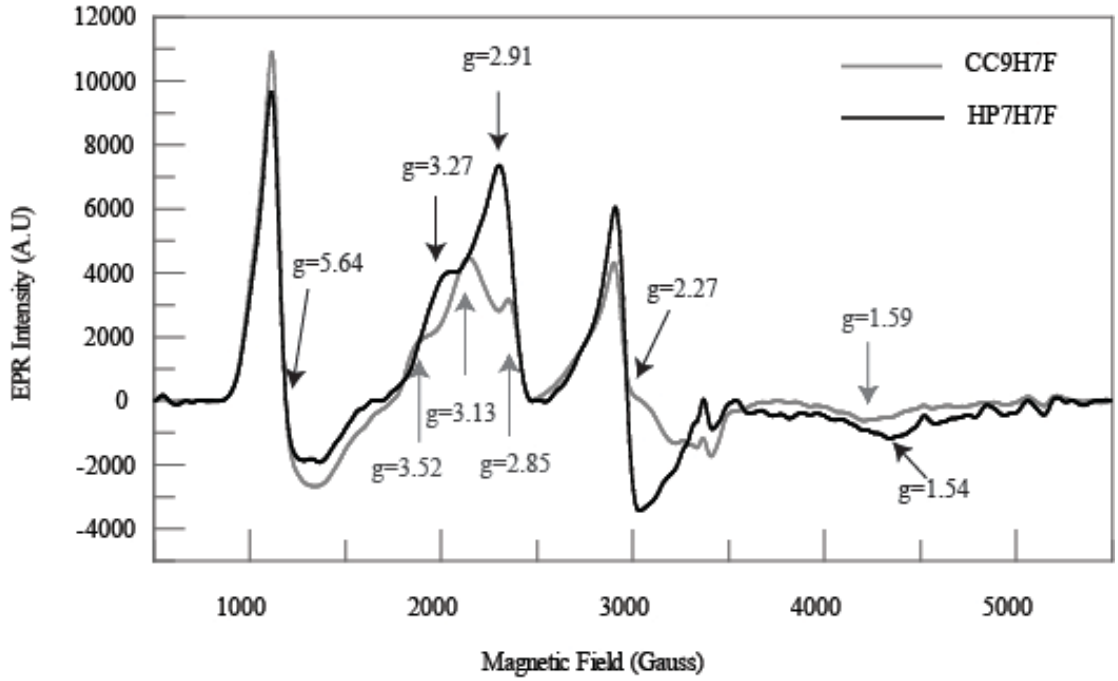

Figure 3.9 Electron paramagnetic resonance (EPR) spectroscopy of CC9H7F and HP7H7F

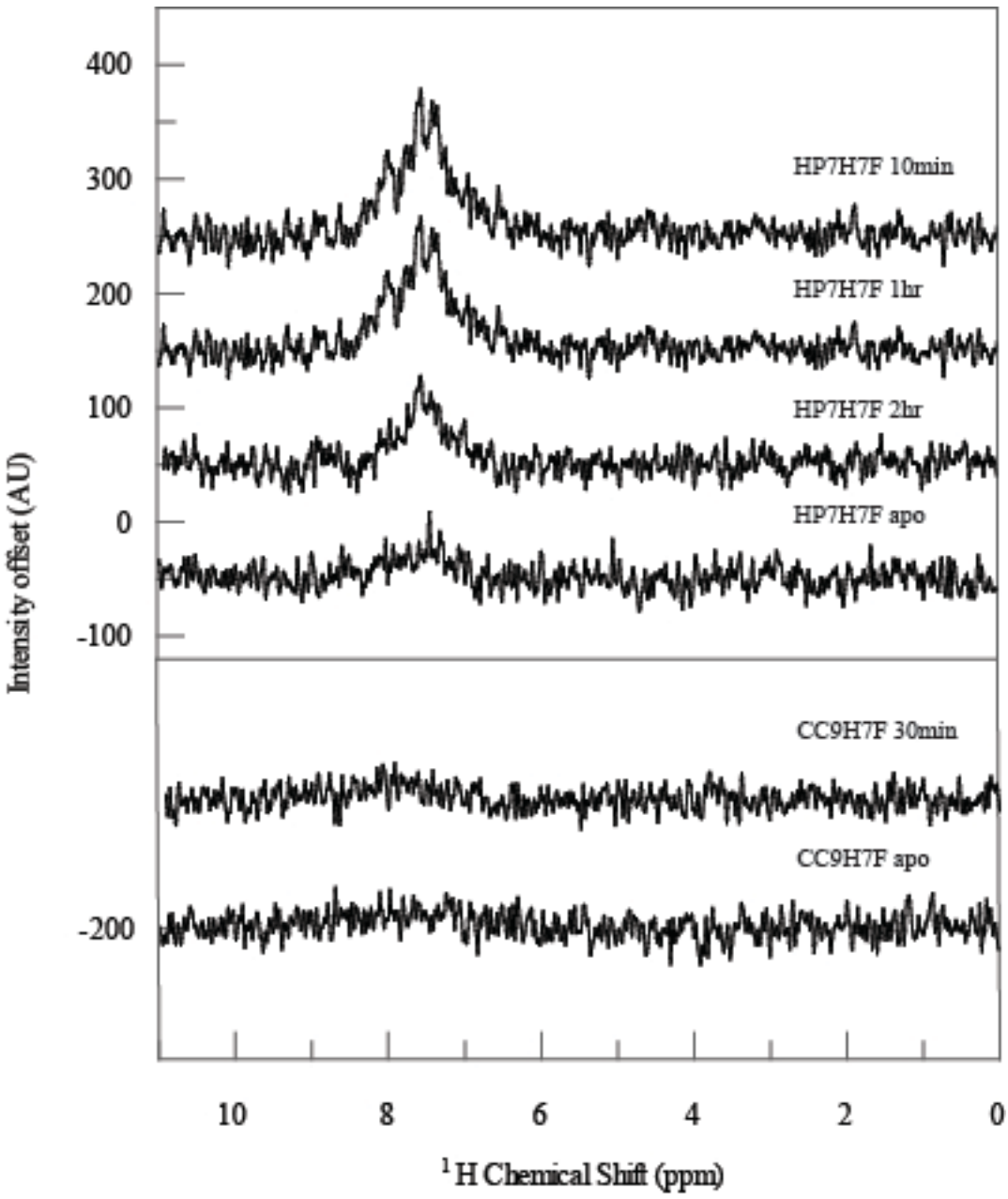

Figure 3.10 NMR determination of Hydrogen-Dueterium exchange rates of the backbone N-H bonds in apo-HP7-H7F, apo-CC9-H7F and heme complex of each protein. 1D N^{15}-HSQC spectra as a function of time, showing the rates of D_2O penetrating into the hydrophobic binding core.

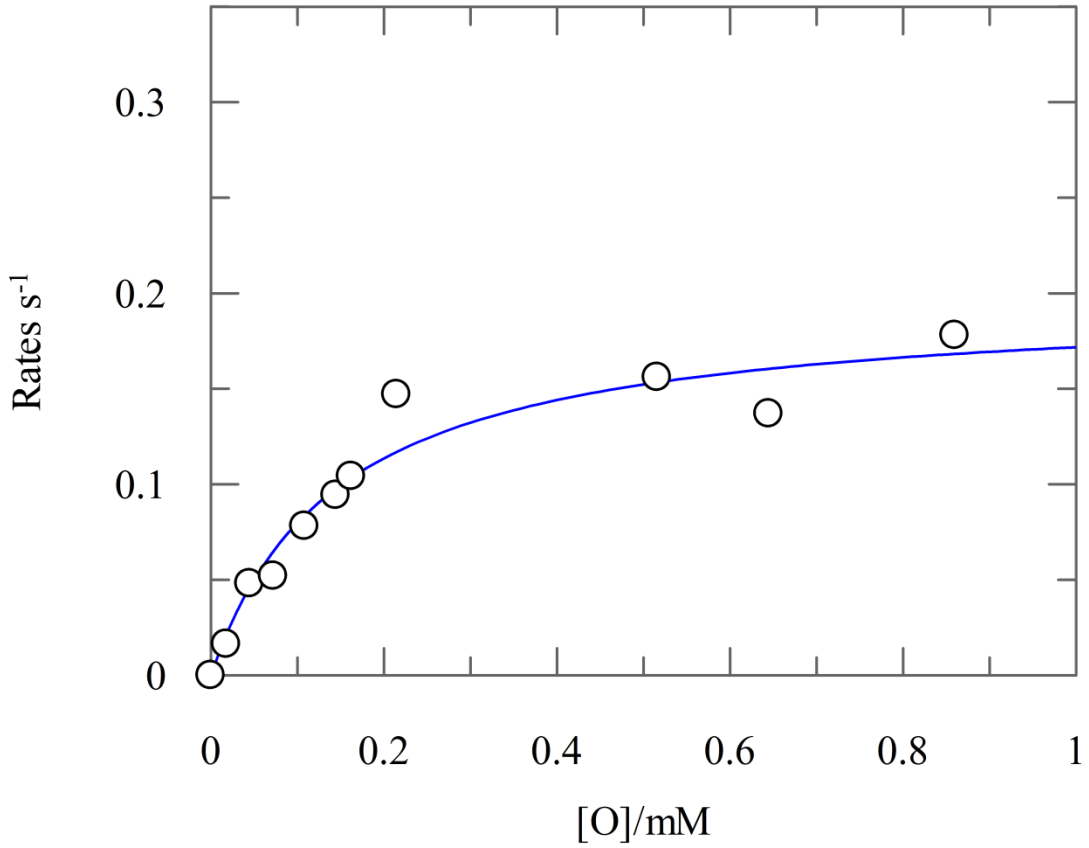

Figure 3.11 Lifetime analysis of O_2 and histidine binding to HP7-H7F. Stopped-flow analysis of the rates of O_2 oxidizing reduced heme proteins as a function of ligand concentration. Lines are fits with eqn.10.

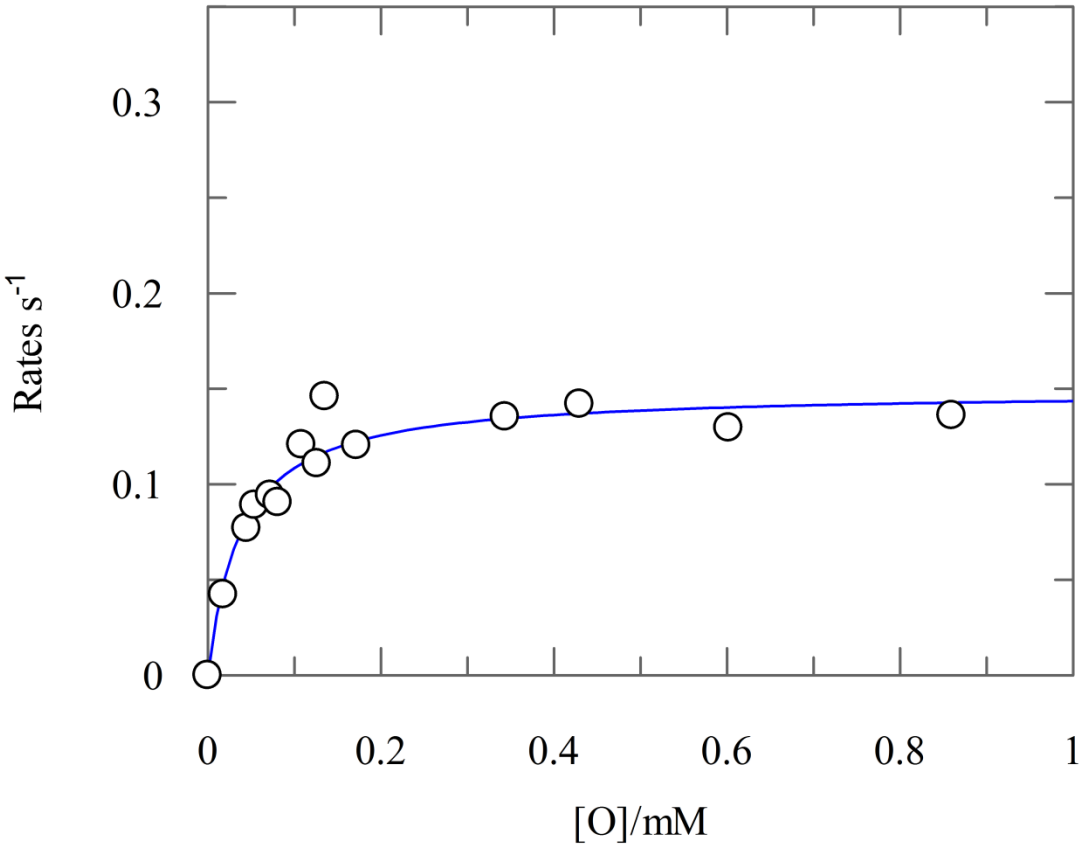

Figure 3.12 Lifetime analysis of O_2 and mono-histidine binding to HP7. Stopped-flow analysis of the rates of O_2 oxidizing reduced heme proteins as a function of ligand concentration. Lines are fits with eqn.10.

Section 3.5: Conclusion

The detailed analysis presented here, of the effects of the mutational manipulation of entactic state energy on gaseous ligand binding properties in our artificial hexacoordinate oxygen transport protein, reveals the fundamental challenges in the design and optimization of a functional protein. Recent progress in the field of protein design has rendered the creation of a natively-structured, high-affinity oxygen-binding protein relatively uncomplicated, but functional transport proteins will necessarily require longer oxygen-binding lifetimes. Early successes in the design of oxygen-binding proteins took advantage of the destabilization of one of two heme-ligating histidine residues, preventing the rapid oxidation of ferrous heme. Increased oxyferrous state lifetimes will also be dependent upon decreased water penetration into the protein core.

Section 3.6: Footnotes

[1]Abbreviations used: CO, carbon monoxide; EPR, electron paramagnetic resonance; HSQC , heteronuclear single quantum coherence; NMR, nuclear magnetic resonance; O_2, molecular oxygen

[2]We have chosen this terminology instead of proximal and distal to avoid confusion of the heme binding site location with the proximal and distal histidine ligand in each binding site.

Section 3.7: Acknowledgements

The authors thank Brian Gibney of the Department of Chemistry, Brooklyn College and Mark Hargrove, of the Department of Biophysics, Iowa State University for many helpful discussions. We thank Hsin Wang, of the Department of Chemistry, the City College of New York, for assistance with NMR measurements. RLK gratefully acknowledges support by the following grants: MCB-0920448 from the National Science Foundation, infrastructure support from P41 GM-66354 to the New York Structural Biology Center and the NIH National Center for Research Resources to CCNY (NIH 5G12 RR03060)c. EMEA gratefully acknowledges support from the CCNY-KTH exchange program supported by the National Science Foundation Grant 0968244.

Section 3.8: Reference

1. Brunori, M., Giuffre, A., and Sarti, P. (2005) Cytochrome c oxidase, ligands and electrons, *Journal Of Inorganic Biochemistry 99*, 324-336.

2. Trent, J. T., Hvitved, A. N., and Hargrove, M. S. (2001) A model for ligand binding to hexacoordinate hemoglobins, *Biochemistry 40*, 6155-6163.

3. Koder, R. L., Anderson, J. L. R., Solomon, L. A., Reddy, K. S., Moser, C. C., and Dutton, P. L. (2009) Design and engineering of an O2 transport protein, *Nature 458*, 305-309.

4. Koder, R. L., Valentine, K. G., Cerda, J. F., Noy, D., Smith, K. M., Wand, A. J., and Dutton, P. L. (2006) Native-like structure in designed four helix bundles driven by buried polar interactions, *Journal of the American Chemical Society 128*, 14450-14451.

5. Vallee, B. L., and Williams, R. J. P. (1968) Metalloenzymes - entatic nature of their active sites, *Proceedings Of The National Academy Of Sciences Of The United States Of America 59*, 498-+.

6. Zhang, L., Anderson, J. L. R., Ahmed, I., Norman, J. A., Negron, C., Mutter, A. C., Dutton, P. L., and Koder, R. L. (2011) Manipulating Cofactor Binding Thermodynamics in an Artificial Oxygen Transport Protein, *Biochemistry 50*, 10254-10261.

7. Moffet, D. A., Case, M. A., House, J. C., Vogel, K., Williams, R. D., Spiro, T. G., McLendon, G. L., and Hecht, M. H. (2001) Carbon monoxide binding by de novo heme proteins derived from designed combinatorial libraries, *Journal of the American Chemical Society 123*, 2109-2115.

8. Spiro, T. G., and Wasbotten, I. H. (2005) CO as a vibrational probe of heme protein active sites, *Journal Of Inorganic Biochemistry 99*, 34-44.

9. Hirota, S., Kishi, M., Yamauchi, O., Wang, Y. H., and Huang, Z. X. (2001) Carbon monoxide complex of cytochrome b(5) at acidic pH, *Biochemical And Biophysical Research Communications 282*, 351-355.

10. Englander, S. W., Calhoun, D. B., and Englander, J. J. (1987) Biochemistry without oxygen, *Anal. Biochem. 161*, 300-306.

11. Hargrove, M. S. (2000) A flash photolysis method to characterize hexacoordinate hemoglobin kinetics, *Biophysical Journal 79*, 2733-2738.

12. Gardner, A. M., Martin, L. A., Gardner, P. R., Dou, Y., and Olson, J. S. (2000) Steady-state and transient kinetics of Escherichia coli nitric-oxide dioxygenase (flavohemoglobin) - The B10 tyrosine hydroxyl is essential for dioxygen binding and catalysis, *J. Biol. Chem. 275*, 12581-12589.

13. Delaglio, F., Grzesiek, S., Vuister, G., Zhu, G., Pfeifer, J., and Bax, A. (1995) NMRPipe: A Multidimensional Spectral Processing System Based on UNIX Pipes, *J. Biomol. NMR 6*, 277-293.

14. Goddard, T. D., and Kneller, D. G. (2207) Sparky, The University of California, San Francisco.

15. Kay, L. E., Keifer, P., and Saarinen, T. (1992) Pure Absorption Gradient Enhanced Heteronuclear Single Quantum Correlation Spectroscopy with Improved Sensitivity, *J. Am. Chem. Soc. 114*, 10663-10665.

16. Ascenzi, P., Bocedi, A., de Sanctis, D., Pesce, A., Bolognesi, M., Marden, M. C., Dewilde, S., Moens, L., Hankeln, T., and Burmester, T. (2004) Neuroglobin and cytoglobin - Two new entries in the hemoglobin superfamily, *Biochemistry and Molecular Biology Education 32*, 305-313.

17. Du, W. H., Syvitski, R., Dewilde, S., Moens, L., and La Mar, G. N. (2003) Solution H-1 NMR characterization of equilibrium heme orientational disorder with functional consequences in mouse neuroglobin, *Journal of the American Chemical Society 125*, 8080-8081.

18. Smagghe, B. J., Halder, P., and Hargrove, M. S. (2008) Measurement of distal histidine coordination equilibrium and kinetics in hexacoordinate hemoglobins, In *Globins and Other Nitric Oxide-Reactive Proteins, Pt A*, pp 359-378, Elsevier Academic Press Inc, San Diego.

19. Li, L., Hsu, A., and Moore, P. K. (2009) Actions and interactions of nitric oxide, carbon monoxide and hydrogen sulphide in the cardiovascular system and in inflammation - a tale of three gases!, *Pharmacology & Therapeutics 123*, 386-400.

20. Ryter, S. W., and Otterbein, L. E. (2004) Carbon monoxide in biology and medicine, *Bioessays 26*, 270-280.

Chapter 4: Bibliography

1. Sheng, H., Yang, W., Fukuda, S., Tse, H. M., Paschen, W., Johnson, K., Batinic-Haberle, I., Crapo, J. D., Pearlstein, R. D., Piganelli, J., and Warner, D. S. (2009) Long-term neuroprotection from a potent redox-modulating metalloporphyrin in the rat, Free Radic. Biol. Med. 47, 917-923.

2. Koder, R. L., and Dutton, P. L. (2006) Intelligent design: the de novo engineering of proteins with specified functions, Dalton Transactions 25, 3045-3051.

3. Lu, Y. (2005) Design and engineering of metalloproteins containing unnatural amino acids or non-native metal-containing cofactors, Current Opinion in Chemical Biology 9, 118-126.

4. Robertson, D. E., Farid, R. S., Moser, C. C., Urbauer, J. L., Mulholland, S. E., Pidikiti, R., Lear, J. D., Wand, A. J., Degrado, W. F., and Dutton, P. L. (1994) Design and Synthesis of Multi-Heme Proteins, Nature 368, 425-431.

5. Choma, C. T., Lear, J. D., Nelson, M. J., Dutton, P. L., Robertson, D. E., and Degrado, W. F. (1994) Design of a Heme-Binding 4-Helix Bundle, Journal of the American Chemical Society 116, 856-865.

6. Cowley, A. B., Kennedy, M. L., Silchenko, S., Lukat-Rodgers, G. S., Rodgers, K. R., and Benson, D. R. (2006) Insight into heme protein redox

potential control and functional aspects of six-coordinate ligand-sensing heme proteins from studies of synthetic heme peptides, Inorganic Chemistry 45, 9985-10001.

7. Reedy, C. J., and Gibney, B. R. (2004) Heme protein assemblies, Chemical Reviews 104, 617-649.

8. Cowley, A. B., and Benson, D. R. (2007) Weak-field anions displace the histidine ligand in a synthetic heme peptide but not in N-acetylmicroperoxidase-8: Possible role of heme geometry differences, Inorganic Chemistry 46, 48-59.

9. Trent, J. T., Hvitved, A. N., and Hargrove, M. S. (2001) A model for ligand binding to hexacoordinate hemoglobins, Biochemistry 40, 6155-6163.

10. Koder, R. L., Anderson, J. L. R., Solomon, L. A., Reddy, K. S., Moser, C. C., and Dutton, P. L. (2009) Design and engineering of an O2 transport protein, Nature 458, 305-309.

11. Anderson, J. L. R., Koder, R. L., Moser, C. C., and Dutton, P. L. (2008) Controlling complexity and water penetration in functional de novo protein design, Biochemical Society Transactions 36, 1106-1111.

12. Koder, R. L., Valentine, K. G., Cerda, J. F., Noy, D., Smith, K. M., Wand, A. J., and Dutton, P. L. (2006) Native-like structure in designed four helix bundles driven by buried polar interactions, Journal of the American Chemical Society 128, 14450-14451.

13. Huang, S. S., Koder, R. L., Lewis, M., Wand, A. J., and Dutton, P. L. (2004) The HP-1 maquette: From an apoprotein structure to a structured hemoprotein designed to promote redox-coupled proton exchange, Proceedings of the National Academy of Sciences of the United States of America 101, 5536-5541.

14. Huang, S. S., Gibney, B. R., Stayrook, S. E., Dutton, P. L., and Lewis, M. (2003) X-ray Structure of a Maquette Scaffold, J. Mol. Biol. 326, 1219-1225.

15. Discher, B. M., Koder, R. L., Moser, C. C., and Dutton, P. L. (2003) Hydrophilic to Amphiphilic Design in Redox Protein Maquettes, *Current Opinion in Chemical Biology 7*, 741-748.

16. Negron, C., Fufezan, C., and Koder, R. L. (2009) Helical Templates for Porphyrin Binding in Designed Proteins, *Proteins-Structure Function And Bioinformatics 74*, 400-416.

17. Hecht, M. H., Das, A., Go, A., Bradley, L. H., and Wei, Y. N. (2004) De novo proteins from designed combinatorial libraries, Protein Science 13, 1711-1723.

18. Kamtekar, S., Schiffer, J. M., Xiong, H. Y., Babik, J. M., and Hecht, M. H. (1993) Protein Design by Binary Patterning of Polar and Nonpolar Amino-Acids, Science 262, 1680-1685.

19. Moffet, D. A., and Hecht, M. H. (2001) De novo proteins from combinatorial libraries, *Chemical Reviews 101*, 3191-3203.

20. Wei, Y. N., Kim, S., Fela, D., Baum, J., and Hecht, M. H. (2003) Solution structure of a de novo protein from a designed combinatorial library, Proceedings of the National Academy of Sciences of the United States of America 100, 13270-13273.

21. Wei, Y. N., Liu, T., Sazinsky, S. L., Moffet, D. A., Pelczer, I., and Hecht, M. H. (2003) Stably folded de novo proteins from a designed combinatorial library, Protein Science 12, 92-102.

22. Vallee, B. L., and Williams, R. J. P. (1968) Metalloenzymes - entatic nature of their active sites, *Proceedings Of The National Academy Of Sciences Of The United States Of America 59*, 498-+.

23. Brunori, M., Giuffre, A., and Sarti, P. (2005) Cytochrome c oxidase, ligands and electrons, *Journal Of Inorganic Biochemistry 99*, 324-336.

24. Pace, C. N., Vajdos, F., Fee, L., Grimsley, G., and Gray, T. (1995) How to Measure and Predict the Molar Absorption-Coefficient of a Protein, Protein Science 4, 2411-2423.

25. Dutton, P. L. (1978) Redox potentiometry: determination of midpoint potentials of oxidation- reduction components of biological electron-transfer systems, Methods in Enzymology 54, 411-435.

26. Andrade, M. A., Chacon, P., Merelo, J. J., and Moran, F. (1993) Evaluation of secondary structure of proteins from UV circular-dichroism spectra using an unsupervised learning neural network, Protein Eng. 6, 383-390.

27. Hargrove, M. S. (2000) A flash photolysis method to characterize hexacoordinate hemoglobin kinetics, Biophysical Journal 79, 2733-2738.

28. Berry, E. A., and Trumpower, B. L. (1987) Simultaneous determination of hemes-A, hemes-B, and hemes-C from pyridine hemochrome spectra, Analytical Biochemistry 161, 1-15.

29. Delaglio, F., Grzesiek, S., Vuister, G., Zhu, G., Pfeifer, J., and Bax, A. (1995) NMRPipe: A Multidimensional Spectral Processing System Based on UNIX Pipes, J. Biomol. NMR 6, 277-293.

30. Goddard, T. D., and Kneller, D. G. (2007) Sparky, The University of California, San Francisco.

31. Kay, L. E., Keifer, P., and Saarinen, T. (1992) Pure Absorption Gradient Enhanced Heteronuclear Single Quantum Correlation Spectroscopy with Improved Sensitivity, J. Am. Chem. Soc. 114, 10663-10665.

32. Pelton, J. G., Torchia, D. A., Meadow, N. D., and Roseman, S. (1993) Tautomeric states of the active-site histidines of phosphorylated and unphosphorylated III(GLC), a signal-transducing protein from escherichia coli, using 2-dimensional heteronuclear NMR techniques, Protein Science 2, 543-558.

33. Nanda, V., and Koder, R. L. (2010) Designing artificial enzymes by intuition and computation, Nature Chemistry 2, 15-24.

34. Lyu, P. C., Liff, M. I., Marky, L. A., and Kallenbach, N. R. (1990) Side-Chain Contributions To The Stability Of Alpha-Helical Structure In Peptides, Science 250, 669-673.

35. Ogihara, N. L., Ghirlanda, G., Bryson, J. W., Gingery, M., DeGrado, W. F., and Eisenberg, D. (2001) Design of three-dimensional domain-swapped dimers and fibrous oligomers, Proceedings Of The National Academy Of Sciences Of The United States Of America 98, 1404-1409.

36. Dunbrack, R. L., and Karplus, M. (1993) Backbone-Dependent Rotamer Library for Proteins - Application to Side-Chain Prediction, Journal of Molecular Biology 230, 543-574.

37. Ascenzi, P., Bocedi, A., de Sanctis, D., Pesce, A., Bolognesi, M., Marden, M. C., Dewilde, S., Moens, L., Hankeln, T., and Burmester, T. (2004) Neuroglobin and cytoglobin - Two new entries in the hemoglobin superfamily, Biochem. Mol. Biol. Educ. 32, 305-313.

38. Du, W. H., Syvitski, R., Dewilde, S., Moens, L., and La Mar, G. N. (2003) Solution H-1 NMR characterization of equilibrium heme orientational disorder with functional consequences in mouse neuroglobin, Journal of the American Chemical Society 125, 8080-8081.

39. Reddi, A. R., Reedy, C. J., Mui, S., and Gibney, B. R. (2007) Thermodynamic investigation into the mechanisms of proton-coupled electron transfer events in heme protein maquettes, Biochemistry 46, 291-305.

40. Reedy, C. J., Kennedy, M. L., and Gibney, B. R. (2003) Thermodynamic characterization of ferric and ferrous haem binding to a designed four-alpha-helix protein, Chemical Communications, 570-571.

41. Skalicky, J. J., Gibney, B. R., Rabanal, F., Urbauer, R. J. B., Dutton, P. L., and Wand, A. J. (1999) Solution structure of a designed four-alpha-helix bundle maquette scaffold, Journal of the American Chemical Society 121, 4941-4951.

42. Sculley, M. J., and Morrison, J. F. (1986) The determination of kinetic constants governing the slow,tight-binding inhibition of enzyme-catalyzed reactions, Biochimica et Biophysica Acta 874, 44-53.

43. Bender, G. M., Lehmann, A., Zou, H., Cheng, H., Fry, H. C., Engel, D., Therien, M. J., Blasie, J. K., Roder, H., Saven, J. G., and DeGrado, W. F. (2007) De novo design of a single-chain diphenylporphyrin metalloprotein, Journal Of The American Chemical Society 129, 10732-10740.

44. Shifman, J. M., Moser, C. C., Kalsbeck, W. A., Bocian, D. F., and Dutton, P. L. (1998) Functionalized de novo designed proteins: Mechanism of proton coupling to oxidation/reduction in heme protein maquettes, *Biochemistry 37*, 16815-16827.

45. Braun, P., Goldberg, E., Negron, C., von Jan, M., Xu, F., Nanda, V., Koder, R. L., and Noy, D. (2011) Design principles for chlorophyll-binding sites in helical proteins, *Proteins-Structure Function And Bioinformatics 79*, 463-476.